biomolecules

MDPI

Review

Hole Transfer and the Resulting DNA Damage

Chryssostomos Chatgilialoglu [1,2,*] and Andrea Peluso [3,*]

[1] Center for Advanced Technologies, Adam Mickiewicz University, 61614 Poznań, Poland
[2] Istituto per la Sintesi Organica e la Fotoreattività, Consiglio Nazionale delle Ricerche, 40129 Bologna, Italy
[3] Dipartimento di Chimica e Biologia "A. Zambelli", Università di Salerno, 84084 Fisciano, Italy
* Correspondence: chrys@isof.cnr.it (C.C.); apeluso@unisa.it (A.P.)

Abstract: In this review, we focus on the one-electron oxidation of DNA, which is a multipart event controlled by several competing factors. We will discuss the oxidation free energies of the four nucleobases and the electron detachment from DNA, influenced by specific interactions like hydrogen bonding and stacking interactions with neighboring sites in the double strand. The formation of a radical cation (hole) which can migrate through DNA (hole transport), depending on the sequence-specific effects and the allocation of the final oxidative damage, is also addressed. Particular attention is given to the one-electron oxidation of ds-ODN containing G:C pairs, including the complex mechanism of the deprotonation vs. hydration steps of a G:C$^{\bullet+}$ pair, as well as to the modes of formation of the two guanyl radical tautomers after deprotonation. Among the reactive oxygen species (ROS) generated in aerobic organisms by cellular metabolisms, several oxidants react with DNA. The mechanism of stable product formation and their use as biomarkers of guanine oxidation in DNA damage are also addressed.

Keywords: DNA; nucleobase; voltammetry; oxidation; radical cation; hole transport; reaction mechanism; oxidative stress; biomarker

1. Introduction

DNA damage can arise from both internal biological processes (endogenous) and external environmental sources (exogenous), with reactive oxygen species (ROS) playing a significant role. A key aspect of oxidatively induced DNA damage is its complexity, e.g., electron detachment occurs primarily at nucleobases and is thermodynamically regulated by their oxidation potentials, which, in turn, depend on the primary and higher order DNA structures; furthermore, the resulting electron hole can migrate along the double strand, and that process can be either under thermodynamic or kinetic control. As a result, over 100 types of lesions have been identified, the majority involving modifications to DNA bases. Thousands of these lesions accumulate within the mammalian cell genome each day. However, DNA repair enzymes effectively remove many of these forms of damage. Some lesions persist and can lead to mutations during cell division. Thus, mutations arise from the combined effects of DNA damage, repair, and replication. The accumulation of mutations can contribute to various diseases, including cancer. For a comprehensive overview of oxidatively induced DNA damage, including quantification methods (in vitro and in vivo), repair mechanisms, and biological consequences, please refer to the two-volume set of books recently published [1].

This review focuses on the mechanistic aspects of one-electron oxidation of DNA and its resulting damage within biomimetic models. We will first discuss the spectroscopic and electrochemical measurements which have been used in the past to elucidate hole

check for updates

Academic Editor: Kouji Hirota

Received: 18 November 2024
Revised: 17 December 2024
Accepted: 19 December 2024
Published: 30 December 2024

Citation: Chatgilialoglu, C.; Peluso, A. Hole Transfer and the Resulting DNA Damage. *Biomolecules* **2025**, *15*, 29. https://doi.org/10.3390/biom15010029

Copyright: © 2024 by the authors. Licensee MDPI, Basel, Switzerland. This article is an open access article distributed under the terms and conditions of the Creative Commons Attribution (CC BY) license (https://creativecommons.org/licenses/by/4.0/).

site energies and long-range charge transport in DNA. Then, we will focus on the fate of the guanine radical cation ($G^{\bullet+}$), the major product of DNA one-electron oxidation, posing particular attention on the mechanisms leading to the formation of some most common lesions.

2. Oxidation Free Energy of Nucleobases

Oxidative damage of DNA is a complex phenomenon controlled by several competing factors of both kinetic and thermodynamic nature. The hole-trapping efficiency of a DNA sequence and the location of the final oxidative damage in the double helix depends on the oxidation free energies of the different nucleobases, which are the primary sites for electron detachment from DNA. The gas-phase ionization energies of DNA nucleobases have been well established for a long time [2,3]. In solution, the oxidation free energies of nucleobases, nucleosides, and nucleotides have been investigated by several techniques: cyclic voltammetry [4,5], photoelectron spectroscopy [6,7], and pulse radiolysis [8,9]. All the methods yield guanine (G) as the most easily oxidizable nucleobase, followed by adenine (A), while cytosine (C) and thymine (T) exhibit significantly higher oxidation free energies. Although almost all techniques respect the above trend, for the ionization levels of DNA constituents in solution, no consensus has been reached. That is mainly because all the employed techniques are unable to provide unambiguous data. Electrochemical measurements are affected by the low solubility of nucleobases, the scarce activity of working electrodes, and narrow electrochemical windows [4,10]; furthermore, nucleobase oxidations are irreversible processes in most solvents used in electrochemistry [5,11], so the electrode response can be affected by unknown collateral reactions. Pulse radiolysis cannot provide a direct measurement of oxidation free energies; the latter are inferred by measuring the rates of electron transfer processes between the sample and a reference system with a known reduction potential. The results will largely depend on the reliability and completeness of the adopted reaction scheme of the redox processes occurring in the solution. Photoelectron spectroscopy allows for the measurement of only the vertical ionization potential (VIP) of a given species; oxidation free energies are then obtained by adding vibrational relaxation energies, which are usually estimated by resorting to theoretical computations in solution. The cumulative error has been estimated to amount to ca. 0.2–0.3 eV.

The inherent difficulties in the measurement of one-electron oxidation potentials of nucleobases by electrochemical methods have sparked a large scientific debate on the reliability of those experimental values. Several computational studies based on either implicit solvation models or hybrid QM/MM solvation schemes have addressed the problem [6,12,13]. However, the approximate nature of such models does not ensure robust quantitative results. Very recently, by combining state-of-the-art ab initio molecular dynamics simulations with a grand-canonical formulation of solutes in aqueous solutions, the oxidation potentials of some nucleobases and related nucleosides have been calculated by explicitly considering the nucleobases immersed into the bulk of solvent molecules (water) treated at full quantum mechanical level [14]. Noteworthy, this state-of-the-art computational study points out that voltammetry estimates of oxidation free energies inferred by raw peak potentials provide very reliable relative hole-site energies for DNA nucleobases, notwithstanding the irreversible nature of nucleobase oxidation in water [14].

3. In Situ Hole Energies in DNA

In DNA, oxidation free energies can be significantly different from single-molecule ones: specific interactions among nucleobases, i.e., hydrogen bonds with their complementary ones in the double helix and with solvent [15–20], as well as stacking interactions with neighboring sites [21–27], significantly affect the oxidation free energies of DNA constituents, making them dependent on the primary and higher-order structure. Because of that, each DNA sequence is characterized by its series of oxidation free energies, often called in situ hole energies [28].

The effects of the formation of H-bonds with a complementary base on the ionization energies of G were first estimated by theoretical computations [15,16] and later on were experimentally observed by Kaway et al. [17], who measured the quenching of the triplet transient absorption of N,N′-Dibutylnaphthaldiimide (NDI) by electron transfer to G and G:C complex, viz.,

$$^{3}\mathrm{NDI}^{*} + \mathrm{G} \rightarrow \mathrm{NDI}^{\bullet -} + \mathrm{G}^{\bullet +} \quad (1)$$

Measurements were carried out in dichloromethane, where the association constants for base pair formation were measured by NMR to be higher than 10^4 M^{-1}, ensuring that a high percentage of guanine derivatives were engaged in the formation of the G:C complex. Nucleosides were properly derivatized with a tert-butyldimethylsilyl group on the ribose unit to increase their solubility in chlorinated organic solvents. The rate of electron transfer (ET) reaction (1) significantly increases for the G:C complex concerning G one, showing that the one-electron oxidation rate of G is controlled by base pairing with C [17,18]. Using the Marcus equation with estimated values of reorganization energy and pre-exponential factors, it was estimated that base pairing lowers the oxidation potential of G by ca. 100 mV [18].

The influence of base pair formation on the oxidation energy of G has also been studied by differential pulse voltammetry using the same silyl derivatives of guanosine (Guo) and deoxycytidine (dCyd) employed by Kawai in chloroform [19]. The results are summarized in Figure 1a. Differential pulse voltammetry showed that for a solution of Guo and dCyd in equimolar quantities, the voltammogram exhibits two well-resolved peaks, with the one at higher voltage attributable to the free fraction of Guo in solution and the other to the formation of the H-bonded base pair. The large shift of the peak potential observed upon base pair formation (0.34 eV) is clearly due to the scarce ability of chloroform to solvate the guanosine cation; in a more polar solvent, the shift is expected to be much lower. Similar results have been found for the H-bonded complex between silyl derivatives of adenosine (Ado′) and deoxythymidine (dThd′); see Figure 1b [20].

The effect of base pair formation on the hole site energies of pyrimidine bases is difficult to investigate using electrochemical techniques because of their higher oxidation potentials. A rough estimate for deoxycytidine has been obtained using spectroelectrochemistry [29]. Spectroelectrochemistry is a powerful technique for investigating the fate of intermediate species produced during an electrochemical process, but, in the event that irreversible redox processes occur, it must be used with great caution: reliable information can be obtained only on condition that all the processes occurring at the electrode are properly identified and their spectra well characterized. The spectroelectrochemistry of Guo in $CHCl_3$, integrated by a careful analysis of the products of the oxidation process, yielded interesting results. Guo oxidation is an irreversible process [19], notwithstanding the electronic absorption spectrum, recorded in an electrochemical cell equipped with an optically transparent thin-layer electrode (OTTLE) under electrolysis at controlled potential, shows the three characteristic absorption peaks of $Guo^{\bullet +}$ in water (320, 390, and 500 nm) [8,30,31]. In DMSO, the electronic absorption spectrum is almost the same as that recorded in an aqueous solution by pulse radiolysis at acidic and neutral pH. In less polar solvents ($CHCl_3$), peak

frequencies are slightly blue-shifted and the intensity of the peak at 310 nm increases as electro-oxidation proceeds, thus suggesting the formation of an oxidation product which absorbs around 300–320 nm. Indeed, upon switching the potential off, only a signal peak at 316 nm persisted. HPLC–MS and NMR allowed for the identification of the oxidation product as a 8-(8-guanosyl)guanosine derivative which exhibits a strong absorption at 320 nm in water [32]. The fact that the radical cation $Guo^{\bullet+}$ is the prevalent species in the electrode during oxidation at controlled potential was also confirmed by the FTIR absorption spectrum of Guo recorded in $CHCl_3$. The difference spectrum (reported in Figure 2b, dashed line) was the same as that obtained by time-dependent spectroscopy and unequivocally assigned to $Guo^{\bullet+}$ [33].

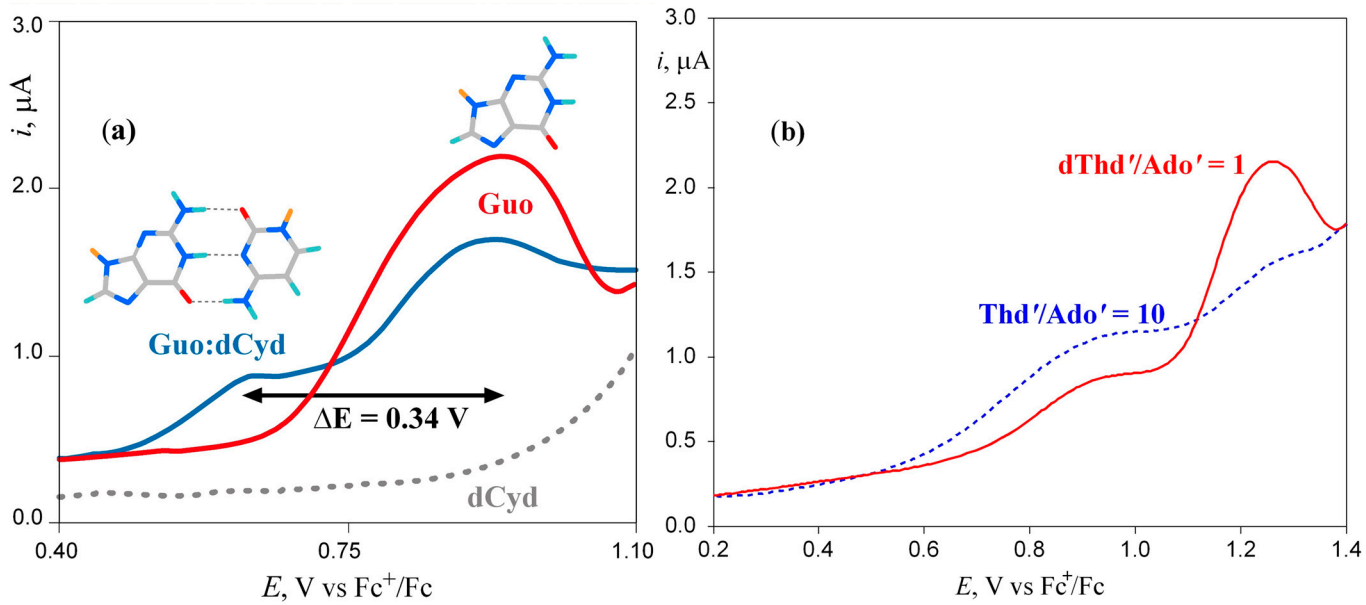


Figure 1. Differential pulse voltammetry of (**a**) 2′,3′-O-isopropylidene 5′-O-(tert-butyldimethylsilyl) guanosine (Guo) (red line), 3′,5′-bis-O-(tertbutyldimethylsilyl)-2′-deoxycytidine (dCyd) (gray dashed line), and their base pair complex Guo:dCyd (blue line) in $CHCl_3$; (**b**) solution containing 2′,3′-O-isopropylidene 5′-O-(tert-butyldimethylsilyl)-adenosine (Ado′) and 3′,5′-bis-O-(tert-butyldimethylsilyl)thymidine (Thd′) in $CHCl_3$, red line Ado′ 2.0 mM and Thd′ 2.0 mM, dashed blue line Ado′ 2.0 mM and Thd′ 20.0 mM. Adapted from refs [19,20] with permission of the American Chemical Society.

The electronic spectra of solutions containing Guo:dCyd mixtures were recorded in an OTTLE cell at a controlled potential of +0.57 V versus Fc^+/Fc in CH_2Cl_2, a condition in which only the complex between the complementary bases can be oxidized. The electronic difference spectrum (with respect to that recorded without any applied potential) exhibits a positive broadband not observed during the oxidation of solutions containing only Guo. The electronic transition was therefore assigned to a charge-transfer transition localizing the hole on the cytidine unit. Indeed, upon replacing dCyd with 5-mCyd, the band was red-shifted by ca. 1200 cm^{-1}, as expected from the fact that the ionization energy of 5-mCyd is lower than that of cytidine by ca. 0.2 eV [3]. Time-dependent density functional theory (TDDFT) computations further supported the above assignment [29]. Those results provided a rough estimate of the vertical ionization energy of dCyd forming the Watson–Crick complex with G.

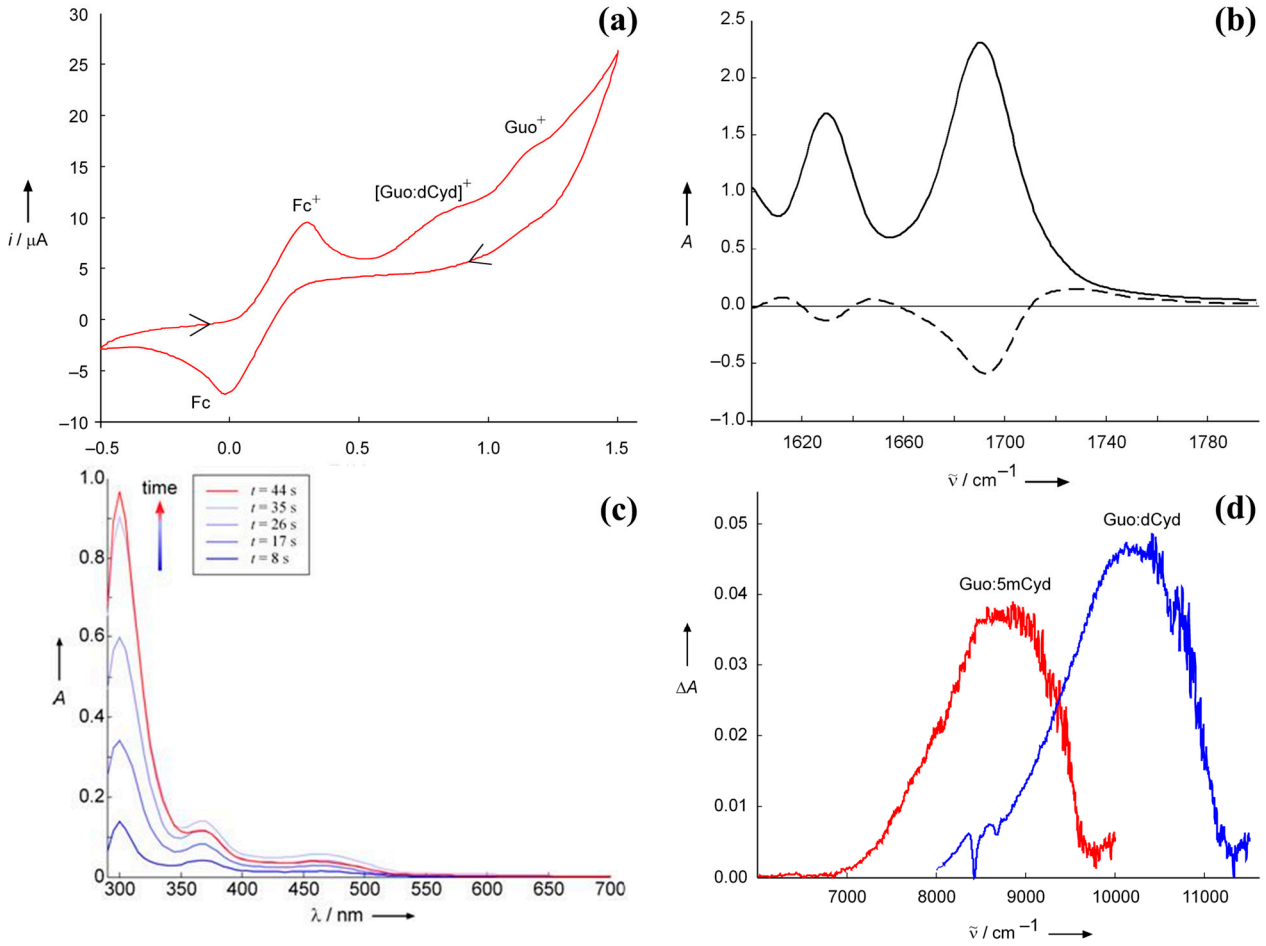


Figure 2. Spectroelectrochemistry characterization of the guanine and cytosine derivatives base pair complex. Panel (**a**): cyclic voltammogram recorded in an OTTLE cell containing 20 mM Guo and 20 mM dCyd in CHCl3; working electrode, Pt, supporting electrolyte tetrabutylammonium perchlorate (TBAP) 0.1 M, scan rate 50 mV/s, ferrocenium/ferrocene (Fc^+/Fc) as internal reference half-couple, arrows show the time variation of the applied potential. Panel (**b**): IR spectrum of guanine in $CHCl_3$, full line, and difference spectrum obtained by subtracting the spectrum of neutral guanine from that recorded at controlled potential (0.91 V vs. Fc^+/Fc), dashed line. Panel (**c**): UV/vis absorption spectral changes recorded during the electro-oxidation at controlled potential of Guo solution 10 mM in chloroform at different times; the intense red curve was recorded after the potential was switched off. Panel (**d**): NIR absorption spectra of the Guo:dCyd base pair complex (black line) and Guo:5mCyd (gray line) complexes in CH_2Cl_2, recorded at +0.57 V vs. Fc^+/Fc. Guo, C: 10 mm; TBAP: 0.1 m; 5mCyd = 2′,3′,5′-tri-O-(tert-butyldimethylsilyl)-5-methylcytidine. Adapted from ref. [29] with permission of Wiley.

Spectroelectrochemical measurements also provided interesting information about the processes occurring during adenosine oxidation at the electrode. The UV-vis and IR spectra of derivativized adenosine in dichloromethane were recorded during potentiostatic oxidation at an optically transparent thin-layer electrode. In the IR region, oxidized Ado shows a broad Zundel-like absorption [34], extending from 2800 up to 3600 cm^{-1}, induced by self-association, possibly followed by PT from the exocyclic amine group of Ado^+ [35]. To the best of our knowledge, no information is currently available for the hole site energy of thymidine H-bonded to its complementary base.

Another important factor that affects hole site energies is intra-strand π–π stacking interactions. Apart from providing the main driving force for the establishment of coiled conformations both in single strand and duplex, intra-strand stacking interactions play

a major role in the chemistry of oxidized DNA [36] because they finely tune the redox potential of the DNA constituents, making them dependent on the primary and higher-order structures [28]. Indeed, DNA oxidative damage exhibits base sequence selectivity: guanines with adjacent purine nucleobases are more reactive than those with adjacent pyrimidine. In particular, GG sequences are more prone to oxidation than GA ones [21–23], and GGG sequences are even more easily oxidizable [24–27].

That observation can be easily rationalized based on the simple but physically sound two-state quantum model: upon the ionization of two consecutive Gs, a G_1G_2 step, two states, $G1^{\bullet+}G2$ and $G_1G_2^{\bullet+}$, which are approximately degenerate, can be formed. If the two Gs are in a stacked configuration, the energies of the two states are shifted compared to unstacked ones by a quantity related to the "strength" of the stacking interaction; see Figure 3 [37].

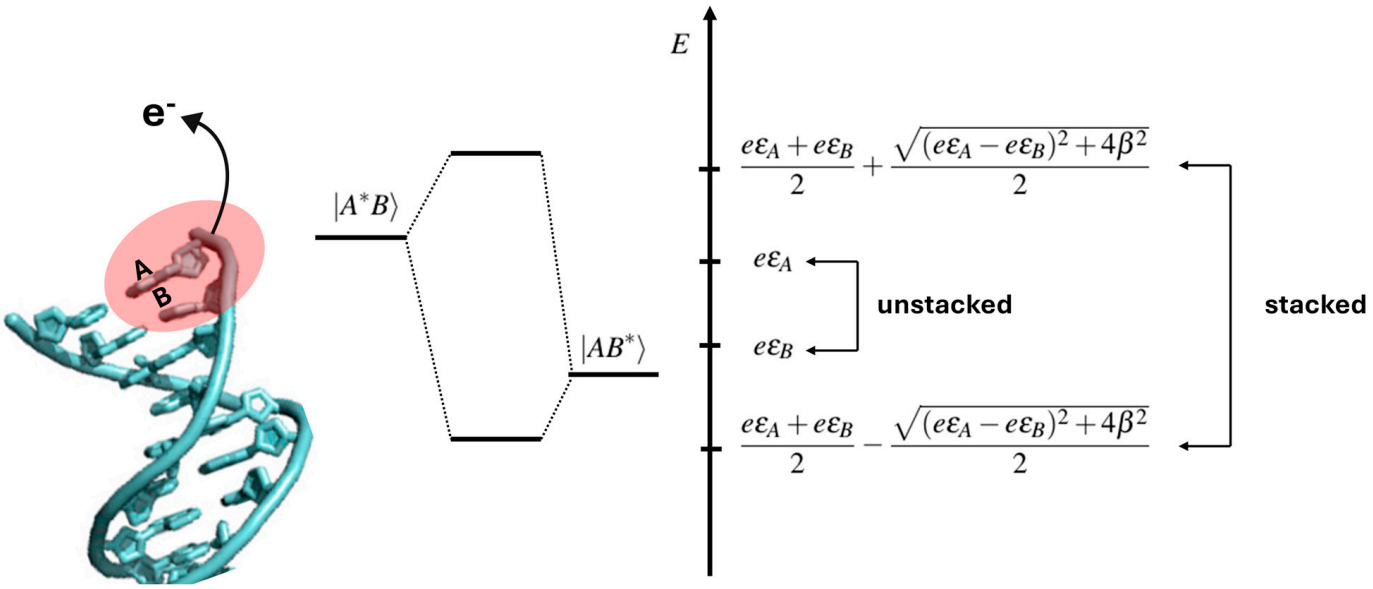


Figure 3. Schematic view showing how π stacking interactions can affect the electronic states of oxidized DNA: a perturbation applied to the A or B unstacked nucleobase, like, for instance, the radiative excitation and/or removal or addition of an electron, leads to two states $|A^*B\rangle$ and $|AB^*\rangle$ with energies ε_A and ε_B. When the same perturbation is applied to A and B π stacked nucleobases, the energy levels of the two states are shifted in energy of an amount which depends on the strength of the π stacking interaction, β, and on the energy difference between ε_A and ε_B (right-side panel). Adapted from ref. [37] with permission of American Chemical Society.

Computational studies yielded results largely in line with the predictions of the simple two-state model and showed that the ionization potential of 5′-GG-3′ is ca. 0.5 eV lower than monomeric 5′-G [38,39]. However, experimental studies have shown that the selectivity observed for oxidative damage at GG or GGG sites compared to single G ones is quite modest [22–24,26], suggesting that either the relative energies of these sites are more similar to each other or that more stable sites are less reactive. Those computational studies neglected the contribution of the solvent reorganization energy. Kurnikov et al. have reported that solvation energies level down oxidation free energies for the calculated gas-phase ionization potentials of G, GG, and GGG sequences. The solvent stabilization energy is larger for a hole localized on a single G and decreases with increasing delocalization. The net effect is a modest stabilization energy, less than 0.1 eV, for GG versus G [40], more in line with the observed oxidative damage selectivity.

Lewis and coworkers approached the problem of stabilization energy due to stacking interactions from a different point of view. They investigated the dynamics of hole transport

in several DNA hairpins possessing a stilbenedicarboxamide electron acceptor and G, GG, and GGG donors and determined the energetics of hole transfer from the observed rates [41,42]. Forward and backward rate constants for photo-induced hole transfer were fitted from time-dependent transient absorption spectroscopical measurements, and the results were employed in a kinetic model for the evaluation of equilibrium constants and free energies for hole transport [42]. GG and GGG donors were found to form slightly deeper hole traps than a single G. The experimental values found for the relative hole free energies of G, GG, and GGG are 0, −0.052, and −0.077 eV [41,42], in line with those estimated by electrochemical measurements; see infra.

Since the strength of π−π stacking interactions is expected to be in the range of 0.1–0.3 eV for a neutral pair [42–44], such an energy difference can be easily detected by differential pulse voltammetry, which is a powerful experimental tool for measuring the sequence dependence of hole site energies in DNA [45]. Indeed, differential pulse voltammetry has provided precious information concerning the effect of stacking interactions on the hole site energies of DNA nucleobases [37]. Excellent reviews and books describing these techniques in detail are available in the literature (see, for instance, reference [46]).

The first voltametric measurements were carried out on A-rich oligonucleotides [37] and only afterward on the more interesting G-rich oligonucleotides [47]. This choice was dictated by the well-known ability of consecutive As to confer structural rigidity to DNA by forming strong stacking interactions [48,49]. Two sets of oligonucleotides were considered, the first one consisting of 5′-ACCCCA-3′ and 5′-AACCAA-3′, the second one including 5′-TTAATT-3′, 5′-TTAAAT-3′, and 5′-TAAAAT-3′ examers, differing for the outer or inner locations of consecutive As inside the oligonucleotide. Differential pulse voltammograms, recorded in water at room temperature with 0.05 M phosphate buffer, showed a lowering of the potential of the first anodic peak as the number of A bases increased for both sets of oligonucleotides. These results were interpreted according to the simple two-state model discussed above in terms of hole delocalization over two or more A nucleobases, in line with previous theoretical computations [50]; see Figure 3. Of note, the above results refer to single-strand oligonucleotides and point toward a well-organized structure of such oligomers in solution due to strong stacking interactions. Computational results suggested that the observed oxidation potential shifts can be assigned to orbital mixing, with a consequent delocalization of the spin density over the stacked nucleobases, leading to the formation of so called delocalized polarons [51,52]. Aside from evidence provided by voltametric measurements, delocalized polarons were also later observed by time-dependent spectroscopy measurements of oxidized DNA hairpins with two or more intervening A-T steps [53].

Similar results have also been obtained for G-rich oligos: a progressive lowering of hole site energies has been observed in examers as the number of consecutive guanines increases. The effect is significant inasmuch as hole site energies can be lowered by 0.3 eV in the case of six consecutive Gs [47]. The effect of hole delocalization in G-rich oligonucleotides is significantly less relevant than in A-rich oligos, in line with the results obtained by transient absorption spectroscopy. Theoretical studies predict that in a GG step, the positive charge is almost entirely localized on 5′-G, probably due to electrostatic interactions [54,55]. Significant hole delocalization has also been found in an alternating GC doubled-stranded oligodeoxynucleotide, i.e., the palindromic 5′-d(GCGCGC)-3′. The oligomer, upon oxidation by $SO_4^{\bullet-}$ produced by ionizing radiation in aqueous solutions under anoxic conditions, exhibits novel time-dependent spectral shapes and kinetic behavior, which were assigned to delocalization of the positive charge over the at least two Gs; see Figure 4 [56]. Although in line with the direct conductance measurements of single DNA oligomers in aqueous solution [57], that

result is somewhat surprising because intra-strand interactions are known to be extremely more effective than inter-strand ones [58].

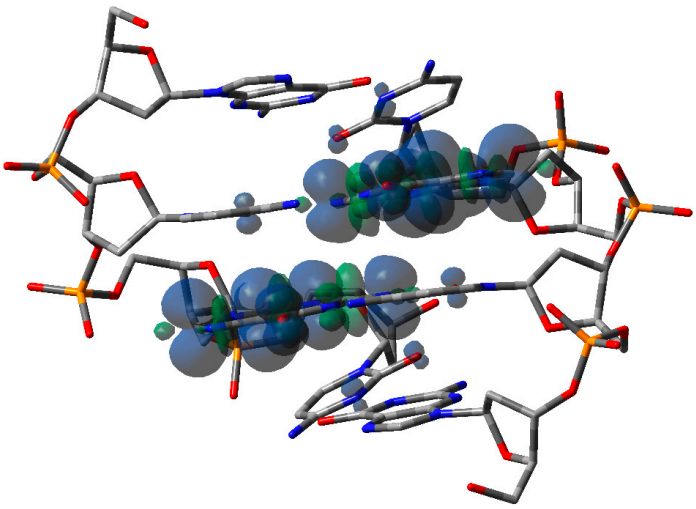


Figure 4. Computed spin density of the optimized structure of one-electron oxidized ds-5′-GCGC-3′. Taken from ref. [56].

Once again, those results suggest that the formation of hole-delocalized domains in DNA is a complex phenomenon where several factors could come into play [40,50,59–62]. Indeed, in DNA, hole solvation energy, which favors charge localization on a single nucleobase, is likely comparable with quantum delocalization energy [40,60], and small factors can tip the scales to one side or the other. This occurs particularly in the case of stacked Gs, for which both time-resolved spectroscopic and electrochemical measurements have shown that hole site energy is slightly affected by delocalization, ca. 0.1 eV [41,42,47]. Contrarily, hole delocalization appears to be favored in tracts of stacked As [37,52], highly favoring charge transport along DNA double strands; see infra [61–63].

4. Charge Transport

The other peculiarity that further complicates the understanding of DNA oxidative damage is the possibility that the radical cation migrates away from the site of its initial formation. Charge transport in duplex DNA was first observed in the late 1960s by Eley and Spivey, who measured the conductivity of some samples of DNA and RNA in the dry state [64]. They suggested that efficient charge transport occurs along paths provided by the stacked aromatic base pairs of duplex DNA. This observation went almost unnoticed until time-dependent spectroscopic observations by Barton and co-workers revealed efficient photoinduced electron transfer over a distance greater than 40 Å, between metal intercalators that are tethered to the 5′ termini of a 15-base pair DNA duplex [65].

This observation triggered a large body of experimental and theoretical studies focused not only on the biologically relevant topic of oxidative DNA damage but also on its potential implications in nanoelectronics, where the self-organizing properties of DNA could be exploited [66–70].

Given the considerations on hole site energies discussed above, charge transport in DNA must strongly depend on the specific sequence of nucleosides and DNA conformation. The sequence dependence of charge (mainly hole) transport has been deeply investigated in DNA oligomers, and several excellent reviews are available in the literature [28,71–75]. It was soon realized that electron transfer (ET) in DNA is extremely different from other ET processes occurring in biosystems because of the tiny energy difference between acceptor and donor groups and because of strong intra-strand interactions between stacked nucleobases

and, probably smaller but still significant, inter-strand interactions [56,63,76,77]. In most of the oligos used for measuring hole transfer rates, the hole is injected into a G site because G is the most easily oxidizable nucleobase, and the acceptor site is usually constituted by GG or GGG steps. As discussed above, the driving force for hole transport in these systems amounts to a few tenths of eV. Furthermore, in studying the distance dependence of hole transfer rates, a bridge of consecutive A:T steps is usually interposed between the donor and acceptor groups. Consecutive A:T steps are the most prone to forming delocalized domains, leading to a significant stabilization of the hole energy. Therefore, increasing hole tunneling distances by increasing the number of interposed A:T steps could also cause a decrease in the energy barrier for hole transport; the two effects could balance each other, leading to a very peculiar regime in which hole transfer rates weakly depend on donor/acceptor distances. A large body of experimental works has clearly shown that ET in DNA is characterized by two regimes, a short range one which exhibits an exponential dependence of the rate on donor/acceptor distances and the other for longer donor/acceptor distances, characterized by a much weaker distance dependence [63,76–84].

Giese's experiment on double-stranded $G(T)_nGGG$ oligos is a good representation of the short- and long-range behavior of hole transfer rates. In that experiment, a hole is injected onto the single G site and the yields of the oxidation products formed at the initial site (P_G) and at the trap site (P_{GGG}) are measured [63]. For oligos containing shorter T sequences, n < 4, the product ratio P_{GGG}/P_G drops by ca. 8 for each interposed T. Vice versa, for n = 4–7, the P_{GGG}/P_G ratio shows a weaker distance dependence, whereas, for n = 7–16, no substantial change in P_{GGG}/P_G ratio is observed. These results suggest that in the short-range regime hole transfer occurs by a coherent super-exchange mechanism, whereas a thermal hopping is operative in the long-range regime [76–84].

In Giese's experiment, the sequence of consecutive A:T steps acts as a shuttle for hole hopping, allowing for efficient electron tunneling up to at least four A:T steps. Curiously, the same structural motif behaves as an unsurmountable barrier for hole transport in other oligomers, studied by Schuster's group, whose structures are reported in Figure 5 [77]; see the caption of Figure 5 for more details.

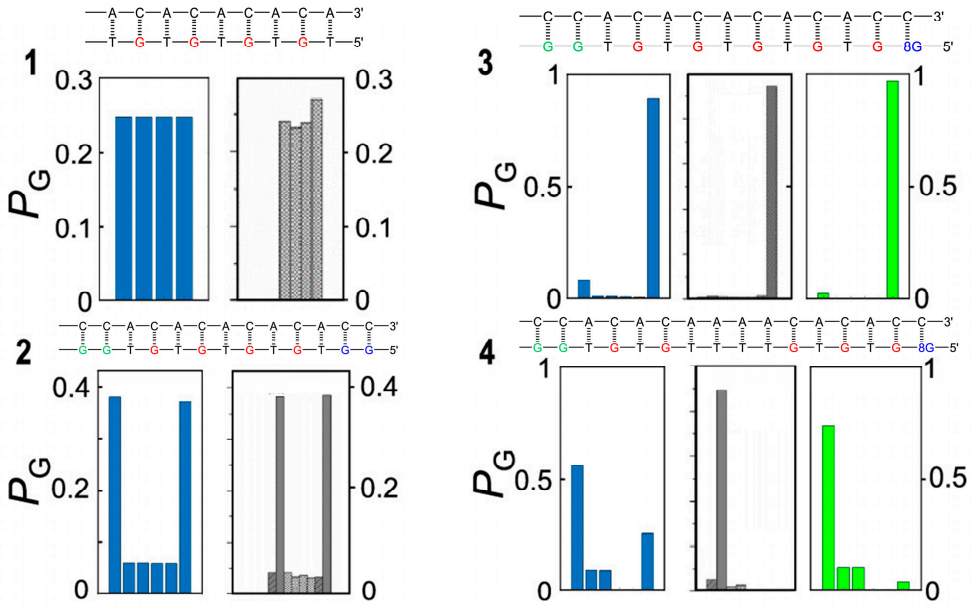


Figure 5. Oligonucleotide sequences and predicted and observed oxidative damage of the four DNA oligomers studied in refs [28,77]. The predicted (blue incoherent and green coherent model) and experimental (gray) product ratios of selective oxidation of the leftmost site are shown in the panel below each oligonucleotide sequence. Oligomer **1** consist only of single G sites and the oxidative damage yield

ratios are almost the same at all G sites. Oligomer **2** contains two trap sites located at the two ends of the sequence; the bridging TGT steps act as very efficient hole shuttles, allowing for easy hole migration along the strand, so that oxidative damage occurs, to a larger extent, at the two trap sites (>80%) and, to a lesser extent, at single G sites. Oligomer **3** possesses a deeper 8-oxo-G trap separated from the leftmost GG site by efficient hole shuttle TGT steps; oxidative damage (>90%) is therefore mainly observed there. Oligomer **4** is characterized by a T quadruplet which separates the donor GG and the acceptor 8-oxo-G sites; the injected hole is not able to freely move along the strand and localizes to a larger extent on the G doublet (>90%) and to a lesser extent on single G's without crossing the T quadruplet bridge. For oligomers 3 and 4, the coherent model yields more satisfying results than the incoherent one, testifying that charge transport cannot occur by a simple sequential hopping mechanism. Adapted from ref [77] with permission American Chemical Society.

This discordant behavior has been recently rationalized by introducing a multistep electron transfer mechanism, in which a manifold of fast coherent elementary ET processes take place in resonance conditions, which are triggered by environmental motions [77,85]. The mechanism is schematized in Figure 6. It essentially consists of four steps: an activation step, which brings a donor and an acceptor group into vibronic degeneracy; step 1, triggering elementary electron transfer between resonant donor and acceptor groups, step 2, which is followed by a relaxation step mainly consisting of solvent relaxation triggered by the nonequilibrium charge distribution created by ET, step 3. The final step consists of the irreversible formation of oxidative damage products, step 4.

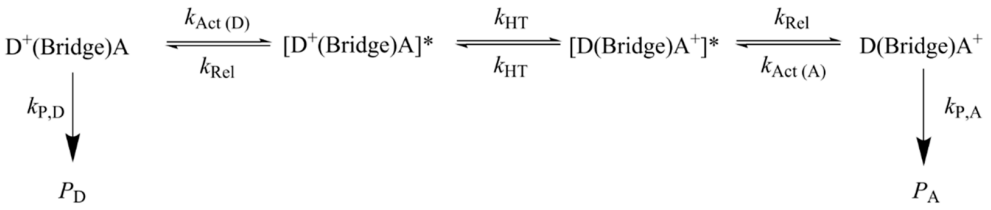


Figure 6. The hole transport mechanism adopted in ref. [77] for predicting the yields of oxidative damage for Giese's ds-G(T)$_n$GGG series and Schuster's oligomers of Figure 5. Star indicates that the donor and acceptor groups are in vibronic resonance.

The ds-G(T)$_n$GGG series of oligomers studied by Giese and coworkers represents a very peculiar case. Simple quantum dynamics simulations showed these are two-state systems, since the time-dependent probability amplitude for hole motion simply oscillates between the donor initial (ground) vibronic state and the final states of the G triplets which are quasi-degenerate with the initial state. Notwithstanding the simplicity of the adopted model—but, what is noteworthy, not that of the computational task, which required the inclusion of a huge number of basis states [86]—the results are in very good agreement with the observed P_{GGG}/P_G, testifying that the essential features of charge transport are caught by the model, on condition that a very large region of the Hilbert space is properly included into computations [87].

By contrast, the set of oligomers considered by Schuster and coworkers contains several sites very close in energy to each other. In this latter case, interference among probability amplitudes could arise, resulting in a much more complex charge transport behavior. Modeling charge transport as an incoherent sequential hopping, in which transient pairwise resonances promote comparatively faster hole motion, provided satisfying results for oligos **1** and **2** in Figure 5. The computed yields of oxidative damage, reported in blue in Figure 5, are in reasonable agreement with the observed one (gray histogram). However, when the incoherent charge transport model is applied to oligos **3** and **4**, significant discordances appear, especially for **4**, for which a significant population, much higher than the observed

one, is predicted on the 8oxo-G trap site; see Figure 5. That result is in line with those obtained for Giese's oligos, which have shown that a bridge of four consecutive T steps works as a shuttle for hole transport, but in **4**, the experimental result is different, and we must accept the experimental observation. These apparent contradictory results were explored in more depth by employing a fully coherent model in which vibronic states of several sites are involved at once for oligos **3** and **4**. In such a model, all the possible low-lying hole sites are brought together in resonant conditions so that the mobile hole can exploit different paths. Such paths interfere with each other, leading to a complex time dependence of probability amplitudes for each site. In this scenario, the kinetic constant to be used in the mechanism of Figure 6 will become time-dependent, making the calculation of the final yields an excessively hard computational task. In ref. [76], the authors chose to feed the kinetic model of Figure 6 with time-independent rate constants obtained by averaging time-dependent rates over a half period of the coherent transition times, i.e., at a complete depopulation of the initial state. This empirical choice led to the computed oxidative damage yields shown in Figure 5, green panel. Now, the computed oxidative damage at the 8oxo-G site is about 1%, in very good agreement with the experimental one and much lower than that yielded by the incoherent model (25%).

The emerging mechanistic picture shares many common points with other mechanisms previously proposed in the literature, such as the flickering resonance charge transport mechanism or the unfurling mechanism [83,84], but, noteworthily, it highlights that coherent effects can manifest themselves even in the presence of fast dephasing mechanisms, a very important feature which characterizes hole transfer in DNA. Indeed, the appearance of coherent effects on macroscopic yield ratios could appear somewhat surprising because of the significantly longer time in which irreversible damage at nucleobases takes place, much longer than coherent hole motion. Solvent deactivation rapidly destroys coherence oscillations, leading to the formation of an equilibrium hole population. That is the case of oligomers **1**, **2**, and, to a lesser extent, **3**. For oligomer 4, the situation is very different; coherent effects have to be empirically considered for reproducing experimental results. Coherent effects lead to the observed formation of two different spatial regions: a kinetically allowed region, within which a quasi-equilibrium population is reached on comparatively longer time scales, and an almost "kinetically forbidden" region, in which hole populations are always too low for establishing an equilibrium regime. The adopted theoretical model works very well for Giese's oligomers, as well as for **1** and **2**, so it would be hard to attribute the poor agreement with experimental data obtained for **4** to its inherent deficiencies. Oligomer **4** has a peculiarity, i.e., the possibility that a given event occurs in different indistinguishable ways which are not present at all in Giese's oligomers or whose effects are less pronounced in **1** and 2. The coherent model takes into account these indistinguishable pathways, yielding more satisfying results, thus suggesting that charge transport in DNA is characterized by different facets that overall cannot be accounted for by a simple sequential hopping mechanism.

5. Deprotonation vs. Hydrolysis of Guanyl Radical Cation ($G^{\bullet+}$): From Nucleoside to DNA

We showed in the previous section that the one-electron oxidation of DNA leads to the guanyl radical cation moiety ($G^{\bullet+}$). The fate of this species follows two main pathways: deprotonation and hydration. The deprotonation process has been studied in detail by various spectroscopic techniques and, in particular, by time-resolved absorption experiments. Figure 7 depicts the H^+ release from the N1 and N2 positions to form G(N1-H) and G(N2-H), respectively. $G(N1\text{-}H)^{\bullet}$ and $G(N2\text{-}H)^{\bullet}$ are two tautomers, and for evidencing

the two tautomeric structures, we draw resonance forms where the unpaired electron is placed in the C5 position [88].

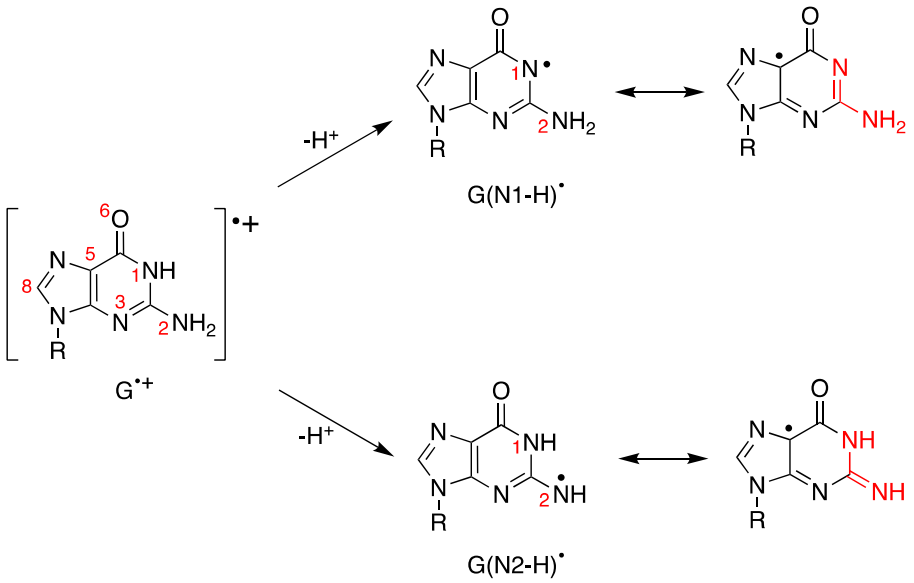


Figure 7. Guanyl radical cation moiety ($G^{\bullet+}$) and the corresponding guanyl radicals G(N1-H)$^{\bullet}$ or G(N2-H)$^{\bullet}$ obtained by loss of protons. Both G(N1-H)$^{\bullet}$ and G(N2-H)$^{\bullet}$ have various resonance forms, including those where the unpaired electron is placed in the C5 position for evidencing the two tautomeric structures (highlighted in red); for more detail, see reference [88].

First of all, the well-understood behavior of guanyl radicals in the building block of DNA, i.e., 2′-deoxyguanosine (dGuo) must be evidenced. The G in dGuo can be oxidized to $G^{\bullet+}$ by a variety of oxidants like $SO_4^{\bullet-}$, $Br_2^{\bullet-}$, $Cl_2^{\bullet-}$, $CO_3^{\bullet-}$ and many others, including various metal complexes [1,88,89]. The subsequent deprotonation exclusively affords G(N1-H)$^{\bullet}$ with a rate constant of 1.5×10^7 s^{-1} and an activation energy of 15.1 ± 1.5 kJ mol^{-1} at pH 7 [90]. The reaction of HO$^{\bullet}$ with dGuo occurs mainly by H-atom abstraction from the exocyclic NH_2 group affording G(N2-H)$^{\bullet}$. The initially formed G(N2-H)$^{\bullet}$ radical undergoes a water-assisted tautomerization with a rate constant of 2.3×10^4 s^{-1} to give the most stable tautomer G(N1-H)$^{\bullet}$ [91,92]. G(N2-H)$^{\bullet}$ has a characteristic band >600 nm that is missing in its tautomer G(N1-H)$^{\bullet}$ [88,91,92]. The replacement of the N1-H moiety with N1-Me results in deprotonation occurring from the exocyclic NH_2 group [8]. Theoretical calculations indicate that deprotonation from the N2-H moiety is competitive with that from the N1-H moiety, with G(N1-H) being favored in environments with high dielectric constants, such as water [93]. In addition, the two conformational isomers of G(N2-H)$^{\bullet}$ in which the remaining N2–H is either *syn* or *anti* to the guanine N3 atom were calculated, revealing that the *syn*-conformer is lower in energy than the *anti*-conformer [93].

The fate of $G^{\bullet+}$ in ds-ODNs or DNA is more complicated [88]. In the early works, it was suggested that in DNA, the proton is not directly released into the aqueous phase but instead remains within the hydrogen-bonded G:$C^{\bullet+}$ pair [89]. ESR studies showed that H^+ is transferred to the adjacent cytosine at 77 K, whereas a prototropic equilibrium should be established at ambient temperature (see the structures highlighted in the colored box in Figure 8) [94]. However, the dynamics of G:$C^{\bullet+}$ pair deprotonation depend strongly on ODN secondary structures. The prototropic equilibria in one electron oxidize G:C, and the subsequent deprotonation step is quite important since it controls the hole transfer in DNA.

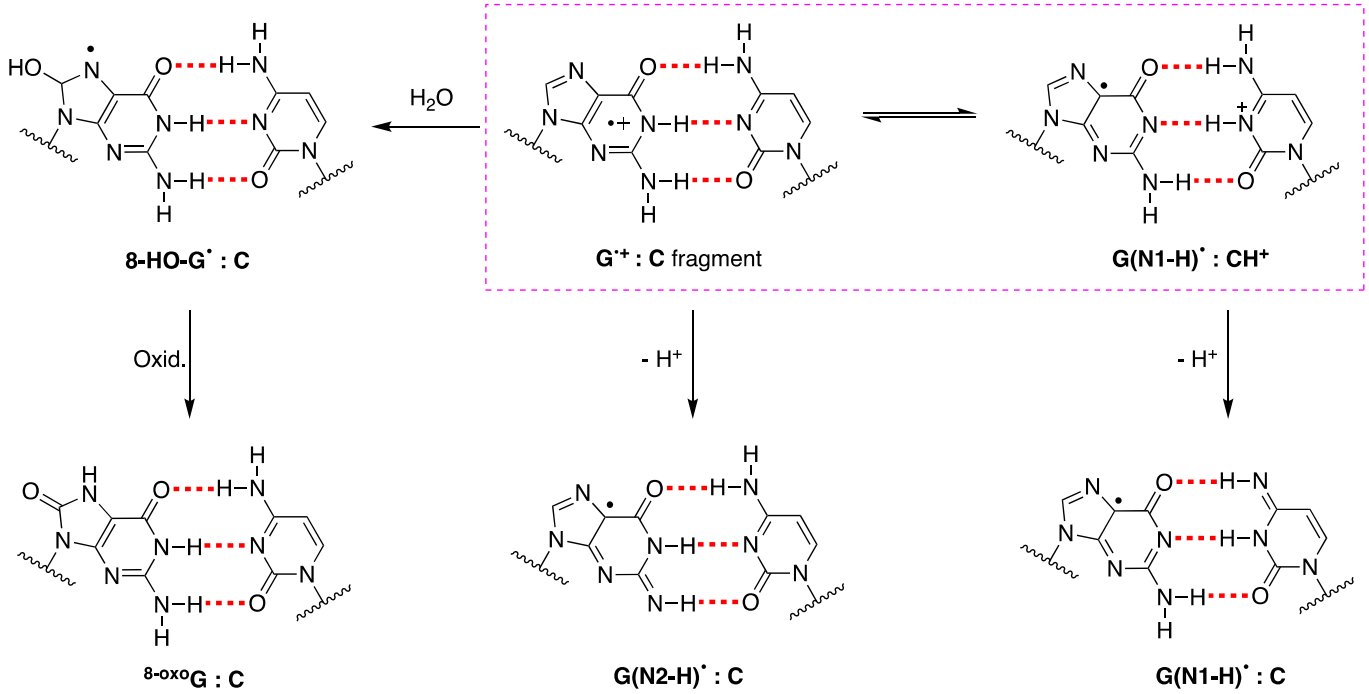


Figure 8. Deprotonation vs. hydration of $G^{\bullet+}$ in ds-ODNs. The fragment $G^{\bullet+}$:C is in equilibrium with G(N1-H)$^{\bullet}$:CH^{+}] and both of them may lose H^{+} affording the two tautomers of guanyl moiety, i.e., G(N2-H)$^{\bullet}$ or G(N1-H)$^{\bullet}$, respectively; the structures of prototropic equilibrium highlighted in the pink dashed box. The hydrolysis of $G^{\bullet+}$ affords 8-HO-G$^{\bullet}$ radical, which follows a further oxidation step to give the $^{8\text{-oxo}}$G:C fragment as a stable product.

The one-electron oxidation of various ds-ODNs containing G:C pairs by $SO_4^{\bullet-}$ has been reported by time-resolved spectroscopies. In the pulse radiolysis study, eleven ds-ODNs with different sequences (11mer to 13mer ds-ODNs) were reported [95]. The monophasic decay of the transient species associated with the release of the proton into solution was observed. The rate constant varied in the range 0.3–2 × 10^7 s^{-1}, depending on the ds-ODN sequence. For example, the transient from the ds-ODN of the 13mer $A_5G_3A_5$ decays with k = 4.5 × 10^6 s^{-1} in water. The proposed mechanism consists of the formation of G(N1-H)$^{\bullet}$:C (see Figure 8). In the laser flash photolysis study, the one-electron oxidation of 30mer ODN 5′-CGT ACT CTT TGG TGG GTC GGT TCT TTC TAT-3′ by $SO_4^{\bullet-}$ was studied in ss-ODNs and ds-ODN [96]. The characteristics and formation of the observed transient species were remarkably consistent in both experimental scenarios and assigned to G(N1-H)$^{\bullet+}$:C. However, the decay kinetics of G(N1-H)$^{\bullet+}$:C differed significantly. In ds-ODN, the decay exhibited a biphasic nature with two distinct lifetimes (~2.2 ms and ~0.18 s), whereas in ss-ODN, the decay was monophasic with a single lifetime of ~0.28 s. The ms decay component in ds-ODN is correlated with a higher yield of 8-oxo-G compared to ss-ODN (see also Section 6).

The deprotonation process of $G^{\bullet+}$ produced by the low-energy/low-intensity photoionization of ODNs was also studied by time-resolved absorption experiments [97–100]. Deprotonation in duplex DNA leads to G(N1-H)$^{\bullet}$ and is completed within 2 μs, whereas in guanine quadruplexes, G(N2-H)$^{\bullet}$ is observed, and it spans from at least 30 ns to over 50 μs; this is connected with the anisotropic structure of DNA and the mobility of its hydration shell.

The alternating guanine cytosine duplexes have attracted considerable interest, obviously due to the multiple G:C pairs that facilitate specific studies. It is reported that the transient species of one-electron oxidation of the 11-mer ds-ODN 5′-d(CGCGCGCGCGC)-3′ release of the proton into solution with a rate constant of 2 × 10^7 s^{-1}, but no data are shown

for this ds-ODN [95]. The ds-ODN d(G*CG*CG*CG*C), where G* is selectively deuterated at C8 on guanine moieties, was used for ESR experiments; it is established that at 77 K, one-electron oxidized guanine in ds-ODN exists in the form of a deprotonated neutral radical G(-H)$^{\bullet}$ due to efficient proton transfer to the hydrogen-bonded cytosine [94]. The transient species generated with the direct absorption of low-energy UV irradiation palindromic ds-ODN sequence 5′-d(GCGCGCGCGC)-3′ and register at 100 µs was assigned at G(N1-H)$^{\bullet}$ [97]. ESR and UV-visible spectroscopy were used to study the one-electron oxidation of the 8-mer ds-ODN d(TGCGCGCA); at pH $\geq$ 7, the initial site of deprotonation was found to be at N1, forming G(N1-H)$^{\bullet}$:C at 155 K, and upon annealing to 175 K, the site of deprotonation to the solvent shifts to an equilibrium mixture of G(N1-H)$^{\bullet}$:C and G(N2-H)$^{\bullet}$:C [101].

As referred above, evidence has suggested that HO$^{\bullet}$ and one-electron oxidants may partly induce common degradation pathways [102]. We recently reported the reaction of $SO_4^{\bullet-}$ and HO$^{\bullet}$ radicals with an alternating GC ds-ODN in aqueous solutions for comparison [56]. In particular, the transient absorption spectra and associated kinetic data in the range of ns to ms were obtained by pulse radiolysis using the palindromic 5′-d(GCGCGC)-3′. The addition of HO$^{\bullet}$ to the G:C pair moiety affording the adduct 8-HO-G$^{\bullet}$:C (k = 2.3 × 10^9 M^{-1} s^{-1} calculated for a G:C pair), whereas the one-electron oxidation by $SO_4^{\bullet-}$ (k = 13.6 × 10^9 M^{-1} s^{-1} calculated for a G:C pair) is different from the previously reported spectra of one-electron oxidation of a variety of ds-ODN after deprotonation, i.e., G(N1-H)$^{\bullet}$:C (Figure 9). The transient spectrum showed a dominant absorption band with λ_{max} = 330 nm, which decayed by a first-order rate constant of 1.5 × 10^5 s^{-1} by hydration affording the 8-HO-G$^{\bullet}$:C adduct. The neutral radical 8-HO-G$^{\bullet}$:C is a common intermediate for both oxidizing species, as illustrated in Figure 9. Computational studies employing density functional theory (DFT) for structural and time-dependent DFT for spectroscopic characterization were conducted on the sequence 5′-d(GCGC)-3′. These studies predicted that the electron-hole is delocalized across the two stacked base pairs, as depicted in Figure 4 [56]. This type of electron-hole stabilization in CG-rich DNA sequences favors reaction with water instead of deprotonation.

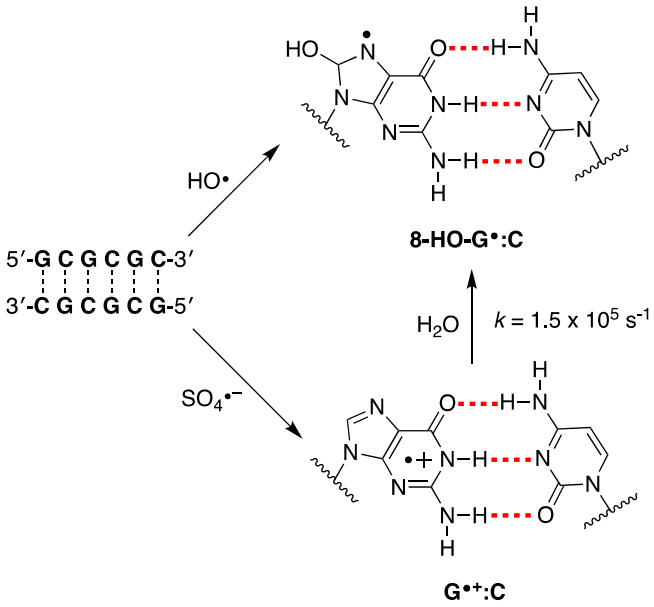


Figure 9. The proposed reaction mechanism for the reaction of HO$^{\bullet}$ and $SO_4^{\bullet-}$ with the double-stranded oligodeoxynucleotide of the palindromic sequence 5′-d(GCGCGC)-3′ in deoxygenated aqueous solutions [56].

A pulse radiolysis study investigated the reaction of a series of 12mer ODNs containing four or two guanines (G), either single-stranded (ss-ODNs) or double-stranded (ds-ODNs), to the reaction with $HO^{\bullet}$ radicals. The characteristic band above 600 nm of guanyl radical G(N2-H)$^{\bullet}$ was observed in ss-ODNs and disappeared on a microsecond timescale but was absent in ds-ODNs [103].

Numerous articles also address the properties of $G^{\bullet+}$:C pair fragments of DNA by theoretical methods, including solvent effects [104–106]. The calculations provide reference absorption spectra for guanine radicals in duplexes and predict changes in transient absorption spectra for hole localization, hydration of the radical cation, and deprotonation steps [97,107]. The separation of charge from spin [G(N1-H)$^{\bullet}$:CH^{+}] and the deprotonation from the exocyclic NH_2 group of cytosine [G(N1-H)$^{\bullet}$:C] were addressed. Additionally, it was predicted that at room temperature, both (G(N1–H)$^{\bullet}$:C and G(N2-H)$^{\bullet}$:C) should exist in equilibrium with nearly equal amounts, as shown by ESR results [101,107]. The reactivity of $HO^{\bullet}$ with the G:C pair was also addressed theoretically by mapping the energy profiles of all possible addition and hydrogen abstraction reactions [56,108,109]. The $HO^{\bullet}$ addition to C8 of G is predicted to be the most favored process. The reactivity of $HO^{\bullet}$ with the triple forming oligonucleotides C(H^{+})G:C favored an ambident reactivity, with the C8 addition leading to 8-HO-G$^{\bullet}$ and the H-abstraction from the NH_2 group leading to G(N2–H)$^{\bullet}$ [110].

6. The Formation Mechanism of the End-Products Used as Biomarkers of Oxidative Stress

Guanine can be oxidized to $G^{\bullet+}$ by various oxidants, including metal complexes. A notable example is the carbonate radical anion ($CO_3^{\bullet-}$), a significant reactive species under physiological conditions. The pair CO_2/HCO_3^{-} functions as an active buffer maintaining physiological pH, with HCO_3^{-} present in millimolar concentrations within the biological environment. Figure 10 illustrates the reaction of CO_2 with peroxynitrite ($ONOO^{-}$) generating $CO_3^{\bullet-}$ through the intermediacy of the unstable nitrosoperoxycarbonate [111,112]. The Fenton reaction, in the presence of HCO_3^{-}, also produces $CO_3^{\bullet-}$ as the predominant species rather than $HO^{\bullet}$ radical [113,114]. The reduction potential of $CO_3^{\bullet-}/CO_3^{2-}$ is 1.59 V. Therefore, $CO_3^{\bullet-}$ is a milder single-electron oxidant that abstracts electrons from guanine moieties [115,116].

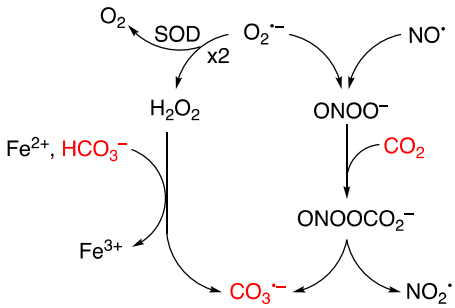


Figure 10. Schematic flow shows the formation of carbonate radical anion ($CO_3^{\bullet-}$) within living organisms. The superoxide radical anion ($O_2^{\bullet-}$) is the primary radical generated in aerobic organisms and serves as the main entry point into the reactive oxygen species (ROS) network. Under physiological conditions, superoxide dismutase (SOD) catalyzes $O_2^{\bullet-}$ to H_2O_2, and $O_2^{\bullet-}$ may react with nitric oxide (NO$^{\bullet}$) to give $ONOO^{-}$. The Fenton reaction in the presence of HCO_3^{-} and the reaction of $ONOO^{-}$ with CO_2 both contribute to the formation of $CO_3^{\bullet-}$.

The main guanine lesions observed in vitro and in vivo from oxidatively generated DNA damage are outlined in Figure 11 [1]. They are collected in two groups: (i) an upper part, with 7,8-dihydro-8-oxo-2′-deoxyguanosine (**8-oxo-G**) and formamidopyrimidine-2′-

deoxyguanosine (**Fapy-G**) characterized by the presence of an open imidazole ring, mainly detected as the free base modification due to stability reasons, and spiroiminodihydantoin (**Sp**) and 5-guanidinohydantoin-2′-deoxyribose (**Gh**), which are further oxidation products of 8-oxo-dG, and (ii) a lower part in the presence of molecular oxygen, with the lesions 5-carboxamido-5-formamido-2- iminohydantoin-2′-deoxyribonucleoside (**2Ih**) and 2-amino-5-[2-deoxyribose]-4H-imidazol-4-one (**Iz**), which rapidly converts to 2,2-diamino-4-[(2- deoxyribose)amino]-5(2H)-oxazolone (**Z**) by hydrolysis. The same end-products are also observed from the oxidation of the building block 2′-deoxyguanosine. However, the different observed distribution of products depends on the substrate, oxidant, and experimental conditions.

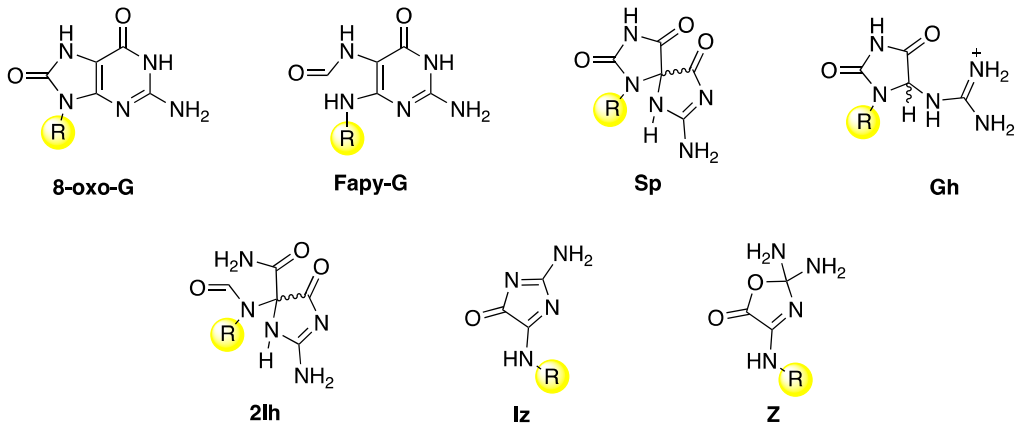


Figure 11. Guanine lesions are detected after oxidatively induced DNA damage in vivo; these lesions are mainly repaired by the base excision repair (BER) pathway. The same lesions have also been found in vitro experiments after reaction with some reactive oxygen species (ROS) through one-electron oxidation and HO$^{\bullet}$ with naked DNA or double-stranded model oligonucleotides or 2′-deoxyguanosine. The substituent R refers to the 2′-deoxyribose moiety.

To discuss the main mechanistic feature of guanine oxidation, Figure 12 shows the reaction of 2′-deoxyguanosine (**G**) by $CO_3^{\bullet-}$ and HO$^{\bullet}$ radicals [88,117,118]. These oxidants give (N1-H)$^{\bullet}$ and 8-HO-G$^{\bullet}$ radicals as common intermediates but are generated by different routes. 8-HO-G$^{\bullet}$ is the common precursor of 8-oxo-G and Fapy-G (Figure 12, upper-left side). Fapy-G formation requires ring-opening followed by one-electron reduction or vice versa (i.e., one-electron reduction followed by ring-opening). The formation of Fapy-G is dependent on the oxygen concentration and the redox environment [119–122]. The reduction potential of 8-oxo-G is 0.55 V lower than that of G [123], and therefore, it is easily oxidized in the presence of one-electron oxidants, affording the by-products Sp and Gh [124,125].

The 8-oxo-G lesions are formed at higher levels in ds-ODNs compared to the other lesions and ss-ODNs. For example, in the one-electron oxidation of 30mer ODNs by $SO_4^{\bullet-}$ study described above, the quantification of the 8-oxo-G lesion as the final product was also measured in both ss-ODNs and ds-ODN [96]. The yield of 8-oxo-G in ds-ODN is ~7 times higher than in ss-ODNs, indicating that the secondary structure of ds-ODN plays an important role. In ds-ODN, the equilibrium [G$^{\bullet+}$:C ⇄ G(N1-H)$^{\bullet}$:CH^{+}] facilitates the hydration with the formation of [8-HO-G$^{\bullet}$:C] that further oxidizes to give the $^{8\text{-oxo}}$G:C (see Figure 8).

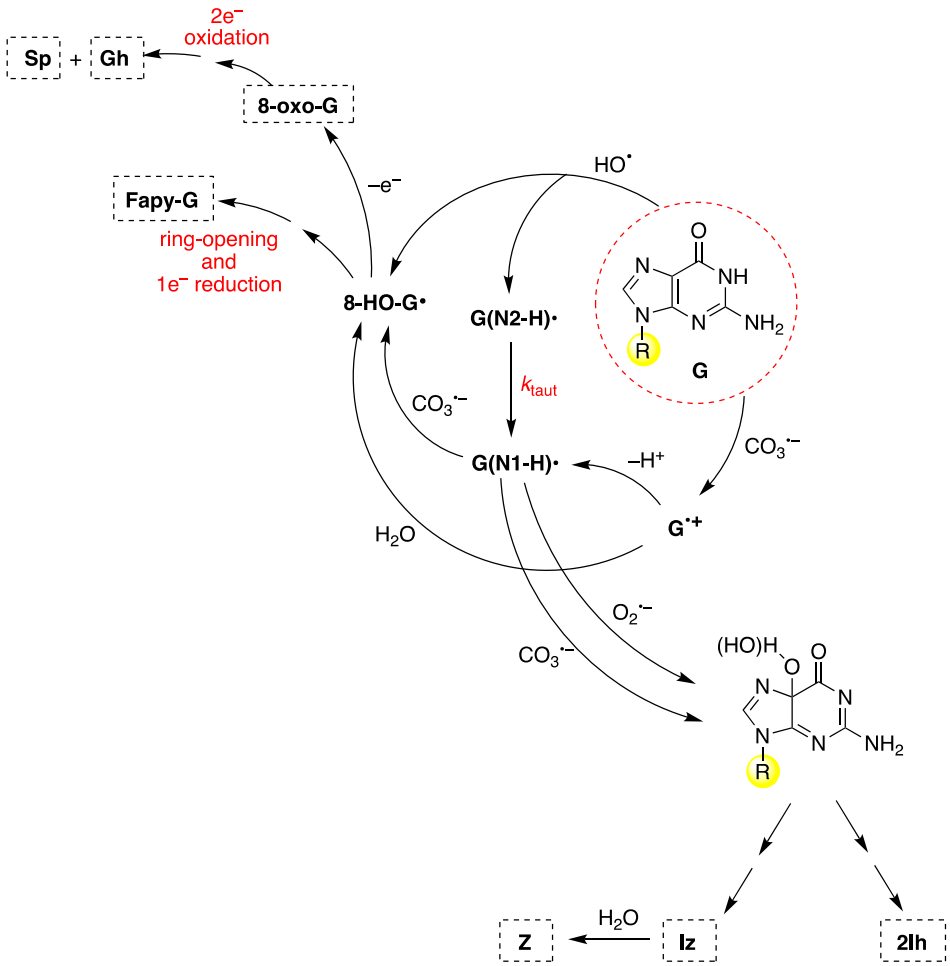


Figure 12. The mechanism of 2′-deoxyguanosine (**G** in the red dashed circle) oxidation by carbonate radical anion ($CO_3^{\bullet-}$) or hydroxyl radical ($HO^{\bullet}$). The substituent R refers to the 2′-deoxyribose moiety. For the chemical structures of the end-products (8-oxo-G, Fapy-G, Sp, Gh, 2Ih, Iz, and Z), see Figure 11.

From the oxidation of G under aerobic conditions or in the presence of $CO_3^{\bullet-}$, two other products are formed via C5 paths (Figure 12, lower-right side), viz., 2Ih and Iz; the latter is further hydrolyzed to Z [126,127]. The oxidation mechanism and kinetics of G by carbonate radical anion ($CO_3^{\bullet-}$) have also been investigated theoretically [128]. Other oxyl-type radicals, like $O_2^{\bullet-}$ and $NO_2^{\bullet}$, react with G(N1-H)$^{\bullet}$ of ss-ODNs or ds-ODNs by combining either C8 or C5 paths (left and right side of Figure 12, respectively) with the formation of the expected end-products [129–131]. A computational investigation into the oxidation of guanine to form Iz through C5 or C8 paths using density functional theory has been reported [132].

A few in vitro studies at a macromolecular level report the simultaneous formation of various lesions using LC-MS/MS and isotopomeric internal standards. For example, a comparative analysis of four oxidized G lesions (8-oxo-G, Sp, Gh, and Z) from the reaction of calf thymus DNA with $ONOO^-$, singlet oxygen derived from photoactivated rose bengal, and $HO^{\bullet}$ radical from γ-radiation was examined [133]. In all cases, the most abundant product was 8-oxo-G, and its accumulation was dependent on the nature of the oxidizing agent with the subsequent conversion to Sp and Gh. Another example is a comparative analysis of three oxidized G lesions (8-oxo-G, Z, and 8-NO_2-G) from the reaction of 18-mer ds-ODNs with $HO^{\bullet}$ from the Fenton reaction or $NO_2^{\bullet}/CO_3^{\bullet-}$ from the decomposition of $ONOOCO_2^-$ (see Figure 10) [134]. Their findings suggest that the patterns of these

lesions' formation in the genome are distinct and are influenced by oxidant identity and the secondary structure of DNA. The oxidatively derived products 2Ih, Sp, and Gh in cellular studies, as well as their recognition by DNA glycosylases and their removal by the base excision repair (BER) pathway, are the focus of a review [135]. Fapy-G, due to its instability, is mainly detected as the free base modification (i.e., Fapy-Gua), and both GC-MS/MS and LC-MS/MS techniques with the isotope dilution approach have been used for measurements in vitro and in vivo [119–121]. It is also worth mentioning that increasing concentrations of oxygen lead to elevated levels of 8-oxo-G in the reaction of $HO^{\bullet}$ with the 21-mer ODN 5′-GGGTTAGGGTTAGG G TTAGGG-3′ in ds-ODN [136,137]. Three pathways lead to the formation of 8-oxo-G in the presence of molecular oxygen: (i) one-electron oxidation (likely via multiple poorly understood reactions) followed by hydration reaction (~45%), (ii) an intramolecular addition of a transiently generated pyrimidine peroxyl radical onto the C8 of a vicinal guanine base (~50%), and (iii) direct addition of $HO^{\bullet}$ to the C8 position of G as the minor path (~5%) [138].

7. Conclusions

In summary, electron detachment from DNA is a complex process influenced by various factors. The resulting radical cation (hole) can migrate through the DNA structure (hole transport). This migration often leads to the formation of a guanyl radical cation ($G^{\bullet+}$) at sites with multiple guanine residues (e.g., GG and GGG sequences). These sequences tend to trap the hole more effectively than single guanine residues. The majority of published research in this area utilizes biomimetic models with tailored oligodeoxynucleotides (ODNs). Within this context, voltametric and spectroelectrochemical measurements have been extensively studied. Recent evidence suggests significant hole delocalization in alternating GC double-stranded oligodeoxynuleotides, where the electron hole is shared across the guanine residues of the two base pairs ($[G:C/C:G]^{\bullet+}$; see Figure 4). Further investigation of this mechanism is anticipated in the near future.

The fate of the $G^{\bullet+}$ radical is also discussed. Specifically, the interplay between deprotonation and hydration pathways of the $G:C^{\bullet+}$ base pair and the mechanisms of product formation are explored. Time-resolved spectroscopic studies and analytical protocols, including LC-MS/MS with isotopomeric internal standards, have been developed to investigate these processes. A variety of guanine lesions have been identified following oxidative DNA damage both in vitro and in vivo. Notably, 8-oxo-G is widely used as a biomarker for oxidative DNA damage. It is estimated that approximately 100–500 guanine bases are oxidized to 8-oxo-G per human cell per day. 8-oxo-G is a mutagenic (miscoding) lesion that can lead to G:C-to-T:A transversion mutations. The repair of guanine lesions primarily involves DNA glycosylases, which initiate the base excision repair (BER) pathway [1]. Biomonitoring of DNA damage, particularly by correlating the levels of various lesions (including guanine lesions) in genomic and mitochondrial DNA samples, will be valuable for a better understanding of oxidative stress in various human diseases and disorders.

Author Contributions: Writing—original draft preparation, C.C. and A.P.; writing—review and editing, C.C. and A.P. All authors have read and agreed to the published version of the manuscript.

Funding: This research received no external funding.

Institutional Review Board Statement: Not applicable.

Informed Consent Statement: Not applicable.

Data Availability Statement: Not applicable.

Acknowledgments: The financial support of the University of Salerno is gratefully acknowledged.

Conflicts of Interest: The authors declare no conflicts of interest.

References

1. Dizdaroglu, M.; Lloyd, R.S. (Eds.) *DNA Damage, DNA Repair and Disease*; Royal Society of Chemistry: Croydon, UK, 2021.
2. Hush, N.S.; Cheung, A.S. Ionization Potentials and Donor Properties of Nucleic Acid Bases and Related Compounds. *Chem. Phys. Lett.* **1975**, *34*, 11–13. [CrossRef]
3. Orlov, V.M.; Smirnov, A.N.; Varshavsky, Y.M. Ionization Potentials and Electron-Donor Ability of Nucleic Acid Bases and Their Analogues. *Tetrahedron Lett.* **1976**, *48*, 4377–4378. [CrossRef]
4. Seidel, C.A.M.; Schulz, A.; Sauer, M.H.M. Nucleobase-Specific Quenching of Fluorescent Dyes. I. Nucleobase One-Electron Redox Potentials and Their Correlation with Static and Dynamic Quenching Efficiencies. *J. Phys. Chem.* **1996**, *100*, 5541–5553. [CrossRef]
5. Oliveira-Brett, A.M.; Piedade, J.A.P.; Silva, L.A.; Diculescu, V.C. Voltammetric Determination of All DNA Nucleotides. *Anal. Biochem.* **2004**, *332*, 321–329. [CrossRef]
6. Schroeder, C.A.; Pluhařov, E.; Seidel, R.; Schroeder, W.P.; Faubel, M.; Slavček, P.; Winter, B.; Jungwirth, P.; Bradforth, S.E. Oxidation Half-Reaction of Aqueous Nucleosides and Nucleotides via Photoelectron Spectroscopy Augmented by ab Initio Calculations. *J. Am. Chem. Soc.* **2015**, *137*, 201–209. [CrossRef] [PubMed]
7. Slavìček, P.; Winter, B.; Faubel, M.; Bradforth, S.E.; Jungwirth, P. Ionization Energies of Aqueous Nucleic Acids: Photoelectron Spectroscopy of Pyrimidine Nucleosides and ab Initio Calculations. *J. Am. Chem. Soc.* **2009**, *131*, 6460–6467. [CrossRef]
8. Candeias, L.P.; Steenken, S. Structure and acid-base properties of one-electron-oxidized deoxyguanosine, guanosine, and 1-methylguanosine. *J. Am. Chem. Soc.* **1989**, *111*, 1094–1099. [CrossRef]
9. Steenken, S.; Jovanovic, S.V. How Easily Oxidizable Is DNA? One-Electron Reduction Potentials of Adenosine and Guanosine Radicals in Aqueous Solution. *J. Am. Chem. Soc.* **1997**, *119*, 617–618. [CrossRef]
10. Faraggi, M.; Broitman, F.; Trent, J.B.; Klapper, M.H. One-Electron Oxidation Reactions of Some Purine and Pyrimidine Bases in Aqueous Solutions. Electrochemical and Pulse Radiolysis Studies. *J. Phys. Chem.* **1996**, *100*, 14751–14761. [CrossRef]
11. Oliveira-Brett, A.M.; Matysik, J.M. Voltammetric and Sonovoltammetric Studies on the Oxidation of Thymine and Cytosine at a Glassy Carbon Electrode. *J. Electroanal. Chem.* **1997**, *429*, 95–99. [CrossRef]
12. D'Annibale, V.; Nardi, A.N.; Amadei, A.; D'Abramo, M. Theoretical Characterization of the Reduction Potentials of Nucleic Acids in Solution. *J. Chem. Theory Comput.* **2021**, *17*, 1301–1307. [CrossRef]
13. Tòth, Z.; Kubečka, J.; Muchov, E.; Slavìček, P. Ionization Energies in Solution with the QM:QM Approach. *Phys. Chem. Chem. Phys.* **2020**, *22*, 10550–10560. [CrossRef]
14. Ambrosio, F.; Landi, A.; Peluso, A.; Capobianco, A. Quantum Chemical Insights into DNA Nucleobase Oxidation: Bridging Theory and Experiment. *J. Chem. Theory Comp.* **2024**, *20*, 9708–9719. [CrossRef]
15. Colson, A.O.; Besler, B.; Sevilla, M.D. Ab Initio Molecular Orbital Calculation of DNA Base Pair Radical Ions: Effects of Base Pairing on Proton Transfer Energies, Electron Affinities and Ionization Potentials. *J. Phys. Chem.* **1992**, *96*, 9787–9794. [CrossRef]
16. Hutter, M.; Clark, T. On the Enhanced Stability of the Guanine−Cytosine Base-Pair Radical Cation. *J. Am. Chem. Soc.* **1996**, *118*, 7574–7577. [CrossRef]
17. Kawai, K.; Wata, Y.; Ichinose, N.; Majima, T. Selective Enhancement of the One-Electron Oxidation of Guanine by Base Pairing with Cytosine. *Angew. Chem. Int. Ed.* **2000**, *39*, 4327–4329. [CrossRef]
18. Kawai, K.; Wata, Y.; Hara, M.; Toyo, S.; Majima, T. Regulation of One-Electron Oxidation Rate of Guanine by Base Pairing with Cytosine Derivatives. *J. Am. Chem. Soc.* **2002**, *124*, 3586–3590. [CrossRef] [PubMed]
19. Caruso, T.; Carotenuto, M.; Vasca, E.; Peluso, A. Direct Experimental Observation of the Effect of the Base Pairing on the Oxidation Potential of Guanine. *J. Am. Chem. Soc.* **2005**, *127*, 15040–15041. [CrossRef] [PubMed]
20. Caruso, T.; Capobianco, A.; Peluso, A. The Oxidation Potential of Adenosine and Adenosine-Thymidine Base-Pair in Chloroform Solution. *J. Am. Chem. Soc.* **2007**, *129*, 15347–15353. [CrossRef]
21. Kovalsky, O.I.; Panyutin, I.G.; Budowsky, E.I. Sequence-Specificity of Alkali-Sensitive Lesions Induced in DNA by High-Intensity Ultraviolet Laser Radiation. *Photochem. Photobiol.* **1990**, *52*, 509–517. [CrossRef]
22. Saito, I.; Takayama, M.; Sugiyama, H.; Nakatani, K. Photoinduced DNA Cleavage via Electron Transfer: Demonstration That Guanine Residues Located 5′ Guanine Are the Most Electron-Donating Sites. *J. Am. Chem.Soc.* **1995**, *117*, 6406–6407. [CrossRef]
23. Muller, J.G.; Hickerson, R.P.; Perez, R.J.; Burrows, C.J. Damage from Sulfite Autoxidation Catalyzed by a Nickel(II) Peptide. *J. Am. Chem. Soc.* **1997**, *119*, 1501–1506. [CrossRef]
24. Nakatani, K.; Fujisawa, K.; Dohno, C.; Nakamura, T.; Saito, I. p-Cyano Substituted 5-Benzoyldeoxyuridine as a Novel Electron-Accepting Nucleobase for One-Electron Oxidation of DNA. *Tetrahedron Lett.* **1998**, *39*, 5995–5998. [CrossRef]
25. Yoshioka, Y.; Kitagawa, Y.; Takano, Y.; Yamaguchi, K.; Nakamura, T.; Saito, I. Experimental and Theoretical Studies on the Selectivity of GGG Triplets toward One-Electron Oxidation in B-Form DNA. *J. Am. Chem. Soc.* **1999**, *121*, 8712–8719. [CrossRef]
26. Hickerson, R.P.; Prat, F.; Muller, J.G.; Foote, C.S.; Burrows, C.J. Sequence and Stacking Dependence of 8-Oxoguanine Oxidation: Comparison of One-Electron vs. Singlet Oxygen Mechanisms. *J. Am. Chem. Soc.* **1999**, *121*, 9423–9428. [CrossRef]

27. Nakatani, K.; Dohno, C.; Saito, I. Modulation of DNA-Mediated Hole-Transport Efficiency by Changing Superexchange Electronic Interaction. *J. Am. Chem. Soc.* **2000**, *122*, 5893–5894. [CrossRef]
28. Kanvah, S.; Joseph, J.; Schuster, G.B.; Barnett, R.N.; Cleveland, C.L.; Landman, U. Oxidation of DNA: Damage to Nucleobases. *Acc. Chem. Res.* **2010**, *43*, 280–287. [CrossRef]
29. Capobianco, A.; Carotenuto, M.; Caruso, T.; Peluso, A. The Charge-Transfer Band of an Oxidized Watson-Crick Guanosine-Cytidine Complex. *Angew. Chem. Int. Ed.* **2009**, *48*, 9526–9528. [CrossRef]
30. Chatgilialoglu, C.; Caminal, C.; Guerra, M.; Mulazzani, Q.G. Tautomers of one-electron oxidized guanosine. *Angew. Chem. Int. Ed.* **2005**, *44*, 6030–6032. [CrossRef]
31. Chatgilialoglu, C.; Caminal, C.; Altieri, A.; Vougioukalakis, G.C.; Mulazzani, Q.G.; Gimisis, T.; Guerra, M. Tautomerism in the guanyl radicals. *J. Am. Chem. Soc.* **2006**, *128*, 13796–13805. [CrossRef] [PubMed]
32. Bose, S.N.; Davies, R.J.H.; Anderson, D.W.; van Niekerk, J.C.; Nassimbeni, L.R.; MacFarlane, R.D. Photochemical (8→8) coupling of purine nucleosides to guanosine. *Nature* **1978**, *271*, 783–784. [CrossRef] [PubMed]
33. Kuimova, M.K.; Cowan, A.J.; Matousek, P.; Parker, A.W.; Sun, X.Z.; Towrie, M.; George, M.W. Monitoring the direct and indirect damage of DNA bases and polynucleotides by using time-resolved infrared spectroscopy. *Proc. Natl. Acad. Sci. USA* **2006**, *103*, 2150–2153. [CrossRef]
34. Zundel, G. Hydrogen bonds with large proton polarizability and proton transfer processes in electrochemistry and biology. *Adv. Chem. Phys.* **2007**, *111*, 1–217.
35. Capobianco, A.; Caruso, T.; Celentano, M.; La Rocca, M.V.; Peluso, A. Proton transfer in oxidized adenosine self-aggregates. *J. Chem. Phys.* **2013**, *139*, 145101. [CrossRef] [PubMed]
36. Schwalb, K.; Temps, F. Base Sequence and Higher-Order Structure Induce the Complex Excited-State Dynamics in DNA. *Science* **2008**, *322*, 243–245. [CrossRef] [PubMed]
37. Capobianco, A.; Caruso, T.; Celentano, M.; D'Ursi, A.M.; Scrima, M.; Peluso, A. Stacking Interactions between Adenines in Oxidized Oligonucleotides. *J. Phys. Chem. B* **2013**, *117*, 8947–8953. [CrossRef] [PubMed]
38. Sugiyama, H.; Saito, I. Theoretical Studies of GG-Specific Photocleavage of DNA via Electron Transfer: Significant Lowering of Ionization Potential and 5′-Localization of HOMO of Stacked GG Bases in B-Form DNA. *J. Am. Chem. Soc.* **1996**, *118*, 7063–7068. [CrossRef]
39. Prat, F.; Houk, K.N.; Foote, C.S. Effect of Guanine Stacking on the Oxidation of 8-Oxoguanine in B-DNA. *J. Am. Chem. Soc.* **1998**, *120*, 845–846. [CrossRef]
40. Kurnikov, I.V.; Tong, G.S.M.; Madrid, M.; Beratan, D.N. Hole Size and Energetics in Double Helical DNA: Competition between Quantum Delocalization and Solvation Localization. *J. Phys. Chem. B* **2002**, *106*, 7–10. [CrossRef]
41. Lewis, F.D.; Liu, X.; Liu, J.; Hayes, R.T.; Wasielewski, M.R. Dynamics and Equilibria for Oxidation of G, GG, and GGG Sequences in DNA Hairpins. *J. Am. Chem. Soc.* **2000**, *122*, 12037–12038. [CrossRef]
42. Lewis, F.D.; Liu, J.; Zuo, Z.; Hayes, R.T.; Wasielewski, M.R. Dynamics and Eergetics of Single-Step Hole Transport in DNA Hairpins. *J. Am. Chem. Soc.* **2003**, *125*, 4850–4861. [CrossRef] [PubMed]
43. Ke, C.; Humeniuk, M.; S-Gracz, H.; Marszalek, P.E. Direct Measurements of Base Stacking Interactions in DNA by Single-Molecule Atomic-Force Spectroscopy. *Phys. Rev. Lett.* **2007**, *99*, 018302. [CrossRef] [PubMed]
44. Cysewski, P.; Czyżnikowska, Ż.; Zaleśny, R.; Czeleń, P. The Post-SCF Quantum Chemistry Characteristics of the Guanine−Guanine Stacking in B-DNA. *Phys. Chem. Chem. Phys.* **2008**, *10*, 2665–2672. [CrossRef]
45. Qi, H.; Chang, J.; Abdelwahed, S.H.; Thakur, K.; Rathore, R.; Bard, A.J. Electrochemistry and Electrogenerated Chemiluminescence of π-Stacked Poly(fluorenemethylene) Oligomers. Multiple, Interacting Electron Transfers. *J. Am. Chem. Soc.* **2012**, *134*, 16265–16274. [CrossRef] [PubMed]
46. Bard, A.J.; Faulkner, L.R.; White, H.S. *Electrochemical Methods: Fundamentals and Application*; Wiley: Hoboken, NJ, USA, 2001.
47. Capobianco, A.; Caruso, T.; D'Ursi, A.M.; Fusco, S.; Masi, A.; Scrima, M.; Chatgilialoglu, C.; Peluso, A. Delocalized Hole Domains in Guanine-Rich DNA Oligonucleotides. *J. Phys. Chem. B* **2015**, *119*, 5462–5466. [CrossRef]
48. El Hassan, M.A.; Calladine, C.R. Conformational Characteristics of DNA: Empirical Classifications and a Hypothesis for the Conformational Behaviour of Dinucleotide Steps. *Philos. Trans. R. Soc. A* **1997**, *355*, 43–100. [CrossRef]
49. Calladine, C.R.; Drew, H.; Luisi, B.; Travers, A. *Understanding DNA: The Molecule and How it Works*, 3rd ed.; Elsevier Academic Press: Oxford, UK, 2004; Chapter 3.
50. Kumar, A.; Sevilla, M.D. Density Functional Theory Studies of the Extent of Hole Delocalization in One-Electron Oxidized Adenine and Guanine Base Stacks. *J. Phys. Chem. B* **2011**, *115*, 4990–5000. [CrossRef] [PubMed]
51. Capobianco, A.; Caruso, T.; Peluso, A. Hole Delocalization over Adenine Tracts in Single Stranded DNA Oligonucleotides. *Phys. Chem. Chem. Phys.* **2015**, *17*, 4750–4756. [CrossRef]
52. Capobianco, A.; Peluso, A. The oxidation potential of AA steps in single strand oligomers. *RSC Adv.* **2014**, *4*, 47887–47893. [CrossRef]

53. Harris, M.A.; Mishra, A.K.; Young, R.M.; Brown, K.E.; Wasielewski, M.R.; Lewis, F.D. Direct Observation of the Hole Carriers in DNA Photoinduced Charge Transport. *J. Am. Chem. Soc.* **2016**, *138*, 5491–5494. [CrossRef] [PubMed]
54. Senthilkumar, K.; Grozema, F.C.; Fonseca Guerra, C.; Bickelhaupt, F.M.; Siebbeles, L.D.A. Mapping the Sites for Selective Oxidation of Guanines in DNA. *J. Am. Chem. Soc.* **2003**, *125*, 13658–13659. [CrossRef]
55. Kumar, A.; Sevilla, M.D. Photoexcitation of Dinucleoside Radical Cations: A Time-Dependent Density Functional Study. *J. Phys. Chem. B* **2006**, *110*, 24181–24188. [CrossRef] [PubMed]
56. Masi, A.; Capobianco, A.; Bobrowski, K.; Peluso, A.; Chatgilialoglu, C. Hydroxyl Radical vs. One-Electron Oxidation Reactivities in an Alternating GC Double-Stranded Oligonucleotide: A New Type Electron Hole Stabilization. *Biomolecules* **2023**, *13*, 1493. [CrossRef] [PubMed]
57. Xu, B.; Zhang, P.; Li, X.; Tao, N. Direct Conductance Measurement of Single DNA Molecules in Aqueous Solution. *Nano Lett.* **2004**, *4*, 1105–1108. [CrossRef]
58. Mallajosyula, S.S.; Pati, S.K. Toward DNA Conductivity: A Theoretical Perspective. *J. Phys. Chem. Lett.* **2010**, *1*, 1881–1894. [CrossRef]
59. Peluso, A.; Caruso, T.; Landi, A.; Capobianco, A. The dynamics of hole transfer in DNA. *Molecules* **2019**, *24*, 4044. [CrossRef]
60. Basko, D.M.; Conwell, E.M. Effect of Solvation on Hole Motion in DNA. *Phys. Rev. Lett.* **2002**, *88*, 098102. [CrossRef] [PubMed]
61. Conwell, E.M.; Bloch, S.M.; McLaughlin, P.M.; Basko, D.M. Duplex Polarons in DNA. *J. Am. Chem. Soc.* **2007**, *129*, 9175–9181. [CrossRef]
62. O'Neill, M.A.; Barton, J.K. DNA Charge Transport: Conformationally Gated Hopping through Stacked Domains. *J. Am. Chem. Soc.* **2004**, *126*, 11471–11483. [CrossRef]
63. Giese, B.; Amaudrut, J.; Köhler, A.K.; Spormann, M.; Wessely, S. Direct Observation of Hole Transfer through DNA by Hopping between Adenine Bases and by Tunneling. *Nature* **2001**, *412*, 318–320. [CrossRef] [PubMed]
64. Eley, D.D.; Spivey, D.I. Semiconductivity of Organic Substances Part 9. Nucleic Acid in Dry State. *Trans. Faraday Soc.* **1962**, *58*, 411–415. [CrossRef]
65. Murphy, C.J.; Arkin, M.R.; Jenkins, Y.; Ghatlia, N.D.; Bossmann, S.H.; Turro, N.J.; Barton, J.K. Long-Range Photoinduced Electron-Transfer through a DNA Helix. *Science* **1993**, *262*, 1025–1029. [CrossRef] [PubMed]
66. Endres, R.G.; Cox, D.L.; Singh, R.R.P. The Quest for High-Conductance DNA. *Rev. Mod. Phys.* **2004**, *76*, 195–214. [CrossRef]
67. Singh, B.; Sariciftci, N.S.; Grote, J.G.; Hopkins, F.K. Bio-Organic-Semiconductor-Field-Effect-Transistor Based on Deoxyribonucleic Acid Gate Dielectric. *J. Appl. Phys.* **2006**, *100*, 024514. [CrossRef]
68. Zalar, P.; Kamkar, D.; Naik, R.; Ouchen, F.; Grote, J.G.; Bazan, G.C.; Nguyen, T.Q. DNA Electron Injection Interlayers for Polymer Light-Emitting Diodes. *J. Am. Chem. Soc.* **2011**, *133*, 11010–11013. [CrossRef] [PubMed]
69. Zhang, Y.; Zalar, P.; Kim, C.; Collins, S.; Bazan, G.C.; Nguyen, T.Q. DNA Interlayers Enhance Charge Injection in Organic Field-Effect Transistors. *Adv. Mater.* **2012**, *24*, 4255–4260. [CrossRef]
70. Gomez, E.F.; Venkatraman, V.; Grote, J.G.; Steckl, A.J. Exploring the Potential of Nucleic Acid Bases in Organic Light Emitting Diodes. *Adv. Mater.* **2015**, *27*, 7552–7562. [CrossRef]
71. Giese, B. Long Distance Electron Transfer through DNA. *Annu. Rev. Biochem.* **2002**, *71*, 51–70. [CrossRef]
72. Lewis, F.D.; Letsinger, R.L.; Wasielewski, M.R. Dynamics of Photoinduced Charge Transfer and Hole Transfer in Synthetic DNA Hairpins. *Acc. Chem. Res.* **2001**, *34*, 159–170. [CrossRef]
73. Genereux, J.C.; Barton, J.K. Mechanisms for DNA Charge Transport. *Chem. Rev.* **2010**, *110*, 1642–1662. [CrossRef] [PubMed]
74. Kawai, K.; Majima, T. Hole Transfer Kinetics of DNA. *Acc. Chem. Res.* **2013**, *46*, 2616–2625. [CrossRef]
75. Arnold, A.R.; Grodick, M.A.; Barton, J.K. DNA Charge Transport: Principles to the Cell. *Cell Chem. Biol.* **2016**, *23*, 183–197. [CrossRef]
76. Landi, A.; Borrelli, R.; Capobianco, A.; Peluso, A. Transient and Enduring Electronic Resonances Drive Coherent Long Distance Charge Transport in Molecular Wires. *J. Phys. Chem. Lett.* **2019**, *10*, 1845–1851. [CrossRef]
77. Landi, A.; Capobianco, A.; Peluso, A. Coherent Effects in Charge Transport in Molecular Wires: Toward a Unifying Picture of Long-Range Hole Transfer in DNA. *J. Phys. Chem. Lett.* **2020**, *11*, 7769–7777. [CrossRef]
78. Bixon, M.; Giese, B.; Wessely, S.; Langenbacher, T.; Michel-Beyerle, M.E.; Jortner, J. Long-Range Charge Hopping in DNA. *Proc. Natl. Acad. Sci. USA* **1999**, *96*, 11713–11716. [CrossRef] [PubMed]
79. Renaud, N.; Berlin, Y.A.; Lewis, F.D.; Ratner, M.A. Between Superexchange and Hopping: An Intermediate Charge-Transfer Mechanism in polyA-polyT DNA Hairpins. *J. Am. Chem. Soc.* **2013**, *135*, 3953–3963. [CrossRef]
80. Renger, T.; Marcus, R.A. Variable Range Hopping Electron Transfer Through Disordered Bridge States: Application to DNA. *J. Phys. Chem. A* **2003**, *107*, 8404–8419. [CrossRef]
81. Bixon, M.; Jortner, J. Incoherent Charge Hopping and Conduction in DNA and Long Molecular Chains. *Chem. Phys.* **2005**, *319*, 273–282. [CrossRef]
82. Grozema, F.C.; Tonzani, S.; Berlin, Y.A.; Schatz, G.C.; Siebbeles, L.D.A.; Ratner, M.A. Effect of Structural Dynamics on Charge Transfer in DNA Hairpins. *J. Am. Chem. Soc.* **2008**, *130*, 5157–5166. [CrossRef] [PubMed]

83. Zhang, Y.; Liu, C.; Balaeff, A.; Skourtis, S.S.; Beratan, D.N. Biological Charge Transfer via Flickering Resonance. *Proc. Natl. Acad. Sci. USA* **2014**, *111*, 10049–10054. [CrossRef]
84. Levine, A.D.; Iv, M.; Peskin, U. Length-Independent Transport Rates in Biomolecules by Quantum Mechanical Unfurling. *Chem. Sci.* **2016**, *7*, 1535–1542. [CrossRef] [PubMed]
85. Leo, A.; Peluso, A. Electron Transfer Rates in Polar and Non-Polar Environments: A Generalization of Marcus' Theory to Include an Effective Treatment of Tunneling Effects. *J. Phys. Chem. Lett.* **2022**, *13*, 9148–9155. [CrossRef] [PubMed]
86. Borrelli, R.; Capobianco, A.; Landi, A.; Peluso, A. Vibronic couplings and coherent electron transfer in bridged systems. *Phys. Chem. Chem. Phys.* **2015**, *17*, 30937–30945. [CrossRef] [PubMed]
87. Borrelli, R.; Di Donato, M.; Peluso, A. Role of intramolecular vibrations in long-range electron transfer between pheophytin and ubiquinone in bacterial photosynthetic reaction centers. *Biophys. J.* **2005**, *89*, 830–841. [CrossRef]
88. Chatgilialoglu, C. The Two Faces of the Guanyl Radical: Molecular Context and Behavior. *Molecules* **2021**, *26*, 3511. [CrossRef] [PubMed]
89. Steenken, S. Purine bases, nucleosides, and nucleotides: Aqueous solution redox chemistry and transformation reactions of their radical cations and e^- and OH adducts. *Chem. Rev.* **1989**, *89*, 503–520. [CrossRef]
90. Zhang, X.; Jie, J.; Song, D.; Su, H. Deprotonation of Guanine Radical Cation $G^{\bullet+}$ Mediated by the Protonated Water Cluster. *J. Phys. Chem. A* **2020**, *124*, 6076–6083. [CrossRef]
91. Chatgilialoglu, C.; D'Angelantonio, M.; Guerra, M.; Kaloudis, P.; Mulazzani, Q.G. A reevaluation of the ambident reactivity of guanine moiety towards hydroxyl radicals. *Angew. Chem. Int. Ed.* **2009**, *48*, 2214–2217. [CrossRef]
92. Chatgilialoglu, C.; D'Angelantonio, M.; Kciuk, G.; Bobrowski, K. New insights into the reaction paths of hydroxyl radicals with 2′-deoxyguanosine. *Chem. Res. Toxicol.* **2011**, *24*, 2200–2206. [CrossRef]
93. Adhikary, A.; Kumar, A.; Becker, D.; Sevilla, M.D. The Guanine Cation Radical: Investigation of Deprotonation States by ESR and DFT. *J. Phys. Chem. B* **2006**, *110*, 24171–24180. [CrossRef] [PubMed]
94. Adhikary, A.; Khanduri, D.; Sevilla, M.D. Direct observation of the hole protonation state and hole localization site in DNA-oligomers. *J. Am. Chem. Soc.* **2009**, *131*, 8614–8619. [CrossRef] [PubMed]
95. Kobayashi, K.; Yamagami, R.; Tagawa, S. Effect of base sequence and deprotonation of guanine cation radical in DNA. *J. Phys. Chem. B* **2008**, *112*, 10752–10757. [CrossRef]
96. Rokhlenko, Y.; Cadet, J.; Geacintov, N.E.; Shafirovich, V. Mechanistic aspects of hydration of guanine radical cations in DNA. *J. Am. Chem. Soc.* **2014**, *136*, 5956–5962. [CrossRef] [PubMed]
97. Banyasz, A.; Martínez-Fernández, L.; Improta, R.; Ketola, T.-M.; Balty, C.; Markovitsi, D. Radicals generated in alternating guanine cytosine duplexes by direct absorption of low-energy UV radiation. *Phys. Chem. Chem. Phys.* **2018**, *20*, 21381–21389. [CrossRef]
98. Balanikas, E.; Banyasz, A.; Baldacchino, G.; Markovitsi, D. Populations and Dynamics of Guanine Radicals in DNA strands—Direct versus Indirect Generation. *Molecules* **2019**, *24*, 2347. [CrossRef]
99. Balanikas, E.; Banyasz, A.; Douki, T.; Baldacchino, G.; Markovitsi, D. Guanine Radicals Induced in DNA by Low-Energy Photoionization. *Acc. Chem. Res.* **2020**, *53*, 1511–1519. [CrossRef]
100. Balanikas, E.; Banyasz, A.; Baldacchino, G.; Markovitsi, D. Deprotonation Dynamics of Guanine Radical Cations. *Photochem. Photobiol.* **2022**, *98*, 523–531. [CrossRef]
101. Adhikary, A.; Kumar, A.; Munafo, S.A.; Khanduri, D.; Sevilla, M.D. Prototropic equilibria in DNA containing one-electron oxidized GC:intra-duplex vs. duplex to solvent deprotonation. *Phys. Chem. Chem. Phys.* **2010**, *12*, 5353–5368. [CrossRef]
102. Cadet, J.; Wagner, J.R. Oxidatively generated base damage to cellular DNA by hydroxyl radical and one-electron oxidants: Similarities and differences. *Arch. Biochem. Biophys.* **2014**, *557*, 47–54. [CrossRef] [PubMed]
103. Chatgilialoglu, C.; Krokidis, M.G.; Masi, A.; Barata-Vallejo, S.; Ferreri, C.; Terzidis, M.A.; Szreder, T.; Bobrowski, K. New insights into the reaction paths of hydroxyl radicals with purine moieties in DNA and double-stranded oligonucleotides. *Molecules* **2019**, *24*, 3860. [CrossRef]
104. Kumar, A.; Sevilla, M.D. Influence of Hydration on Proton Transfer in the Guanine—Cytosine Radical Cation ($G^{\bullet+}$—C) Base P air: A Density Functional Theory Study. *J. Phys. Chem. B* **2009**, *113*, 11359–11361. [CrossRef] [PubMed]
105. Steenken, S.; Reynisson, J. DFT calculations on the deprotonation site of the one-electron oxidised guanine–cytosine base pair. *Phys. Chem. Chem. Phys.* **2010**, *12*, 9088–9093. [CrossRef] [PubMed]
106. Cerón-Carrasco, J.P.; Requena, A.; Perpète, E.A.; Michaux, C.; Jacquemin, D. Theoretical Study of the Tautomerism in the One-Electron Oxidized Guanine-Cytosine Base Pair. *J. Phys. Chem. B* **2010**, *114*, 13439–13445. [CrossRef]
107. Kumar, A.; Sevilla, M.D. Excited States of One-Electron Oxidized Guanine-Cytosine Base Pair Radicals: A Time Dependent Density Functional Theory Study. *J. Phys. Chem. A* **2019**, *123*, 3098–3108. [CrossRef] [PubMed]
108. Zhang, R.; Eriksson, L.A. Effects of OH Radical Addition on Proton Transfer in the Guanine-Cytosine Base Pair. *J Phys. Chem. B* **2007**, *111*, 6571–6576. [CrossRef] [PubMed]
109. Cerón-Carrasco, J.P.; Jacquemin, D. Interplay between hydroxyl radical attack and H-bond stability in guanine–cytosine. *RCS Adv.* **2012**, *2*, 11867–11875. [CrossRef]

110. Wang, Y.; Wei, S. Influence of hydrogen bonds on the reaction of guanine and hydroxyl radical: DFT calculations in C(H^+)GC motif. Phys. *Chem. Chem. Phys.* **2024**, *26*, 5683–5692. [CrossRef] [PubMed]
111. Pacher, P.; Beckman, J.S.; Liaudet, L. Nitric oxide and peroxynitrite in health and disease. *Physiol. Rev.* **2007**, *87*, 315–424. [CrossRef] [PubMed]
112. Möller, M.N.; Denicola, A. Diffusion of peroxynitrite, its precursors, and derived reactive species, and the effect of cell membranes. *Redox Biochem. Chem.* **2024**, *9*, 100033. [CrossRef]
113. Illes, E.; Patra, S.G.; Marks, V.; Mizrahi, A.; Meyerstein, D. The FeII(citrate) Fenton reaction under physiological conditions. *J. Inorg. Biochem.* **2020**, *206*, 111018. [CrossRef]
114. Bounds, P.L.; Koppenol, W.H. Peroxynitrite: A tale of two radicals. *Redox Biochem. Chem.* **2024**, *10*, 100038.
115. Shafirovich, V.; Dourandin, A.; Huang, W.; Geacintov, N.E. The carbonate radical is a site-selective oxidizing agent of guanine in double-stranded oligonucleotides. *J. Biol. Chem.* **2001**, *276*, 24621–24626. [CrossRef]
116. Crean, C.; Geacintov, N.E.; Shafirovich, V. Oxidation of Guanine and 8-oxo-7,8-Dihydroguanine by Carbonate Radical Anions: Insight from Oxygen-18 Labeling Experiments. *Angew. Chem. Int. Ed.* **2005**, *44*, 5057–5060. [CrossRef] [PubMed]
117. Fleming, A.M.; Burrows, C.J. Iron Fenton oxidation of 2′-deoxyguanosine in physiological bicarbonate buffer yields products consistent with the reactive oxygen species carbonate radical anion not hydroxyl radical. *Chem. Commun.* **2020**, *56*, 9779–9782. [CrossRef]
118. Fleming, A.M.; Burrows, C. Chemistry of ROS-mediated oxidation to the guanine base in DNA and its biological consequences. *Int. J. Radiat. Biol.* **2022**, *98*, 452–460. [CrossRef] [PubMed]
119. Jaruga, P.; Kirkali, G.; Dizdaroglu, M. Measurement of formamidopyrimidines in DNA. *Free Radic. Biol. Med.* **2008**, *45*, 1601–1609. [CrossRef] [PubMed]
120. Dizdaroglu, M.; Kirkali, G.; Jaruga, P. Formamidopyrimidines in DNA: Mechanisms of formation, repair, and biological effects. *Free. Radic. Biol. Med.* **2008**, *45*, 1610–1621. [CrossRef] [PubMed]
121. Dizdaroglu, M. Oxidatively induced DNA damage and its repair in cancer. *Mutat. Res. Rev. Mutat. Res.* **2015**, *763*, 212–245. [CrossRef]
122. Greenberg, M.M. The formamidopyrimidines: Purine lesions formed in competition with 8-oxopurines from oxidative stress. *Acc. Chem. Res.* **2012**, *45*, 588–597. [CrossRef]
123. Steenken, S.; Jovanovic, S.V.; Bietti, M.; Bernhard, K. The trap depth (in DNA) of 8-oxo-7,8-dihydro-2′deoxyguanosine as derived from electron-transfer equilibria in aqueous solution. *J. Am. Chem. Soc.* **2000**, *122*, 2373–2374. [CrossRef]
124. Fleming, A.M.; Muller, J.G.; Dlouhy, A.C.; Burrows, C.J. Structural context effects in the oxidation of 8-oxo-7,8-dihydro-2′-deoxyguanosine to hydantoin products: Electrostatics, base stacking, and base pairing. *J. Am. Chem. Soc.* **2012**, *134*, 15091–15102. [CrossRef] [PubMed]
125. Chabot, M.B.; Fleming, A.M.; Burrows, C.J. Insights into the 5-carboxamido-5-formamido-2-iminohydantoin structural isomerization equilibria. *J. Org. Chem.* **2022**, *87*, 11865–11870. [CrossRef]
126. Fleming, A.M.; Muller, J.G.; Ji, I.; Burrows, C.J. Characterization of 2′-deoxyguanosine oxidation products observed in the Fenton-like system Cu(II)/H2O2/reductant in nucleoside and oligodeoxynucleotide contexts. *Org. Biomol. Chem.* **2011**, *9*, 3338–3348. [CrossRef] [PubMed]
127. Alshykhly, O.R.; Fleming, A.M.; Burrows, C.J. 5-Carboxamido-5-formamido-2-iminohydantoin, in Addition to 8-oxo-7,8-Dihydroguanine, Is the Major Product of the Iron-Fenton or X-ray Radiation-Induced Oxidation of Guanine under Aerobic Reducing Conditions in Nucleoside and DNA Contexts. *J. Org. Chem.* **2015**, *80*, 6996–7007. [CrossRef]
128. Wang, Y.; An, P.; Li, S.; Zhou, L. The oxidation mechanism and kinetics of 2′-deoxyguanosine by carbonate radical anion. *Chem. Phys. Lett.* **2020**, *739*, 136982. [CrossRef]
129. Misiaszek, R.; Crean, C.; Joffe, A.; Geacintov, N.E.; Shafirovich, V. Oxidative DNA damage associated with combination of guanine and superoxide radicals and repair mechanisms via radical trapping. *J. Biol. Chem.* **2004**, *279*, 32106–32115. [CrossRef]
130. Misiaszek, R.; Crean, C.; Geacintov, N.E.; Shafirovich, V. Combination of Nitrogen Dioxide Radicals with 8-Oxo-7,8-dihydroguanine and Guanine Radicals in DNA: Oxidation and Nitration End-Products. *J. Am. Chem. Soc.* **2005**, *127*, 2191–2200. [CrossRef]
131. Joffe, A.; Mock, S.; Yun, B.H.; Kolbanovskiy, A.; Geacintov, N.E.; Shafirovich, V. Oxidative Generation of Guanine Radicals by Carbonate Radicals and Their Reactions with Nitrogen Dioxide to Form Site Specific 5-Guanidino-4-nitroimidazole Lesions in Oligodeoxynucleotides. *Chem. Res. Toxicol.* **2003**, *16*, 966–973. [CrossRef]
132. Hebert, S.P.; Bernhard Schlegel, H.B. Computational Investigation into the Oxidation of Guanine to Form Imidazolone (Iz) and Related Degradation Products. *Chem. Res. Toxicol.* **2020**, *33*, 1010–1027. [CrossRef]
133. Cui, L.; Ye, W.; Prestwich, E.G.; Wishnok, J.S.; Taghizadeh, K.; Dedon, P.C.; Tannenbaum, S.R. Comparative analysis of four oxidized guanine lesions from reactions of DNA with peroxynitrite, single oxygen, and γ-radiation. *Chem. Res. Toxicol.* **2013**, *26*, 195–202. [CrossRef]

134. Matter, B.; Seiler, C.L.; Murphy, K.; Ming, X.; Zhao, J.; Lindgren, B.; Jones, R.; Tretyakova, N. Mapping three guanine oxidation products along DNA following exposure to three types of reactive oxygen species. *Free Radic. Biol. Med.* **2018**, *121*, 180–189. [CrossRef] [PubMed]
135. Fleming, A.M.; Burrows, C.J. Formation and processing of DNA damage substrates for the hNEIL enzymes. *Free Radic. Biol. Med.* **2017**, *107*, 35–52. [CrossRef]
136. Chatgilialoglu, C.; Eriksson, L.A.; Krokidis, M.G.; Masi, A.; Wang, S.-D.; Zhang, R. Oxygen dependent purine lesions in double-stranded oligodeoxynucleotides: Kinetic and computational studies highlight the mechanism for 5′,8-cyclopurine formation. *J. Am. Chem. Soc.* **2020**, *142*, 5825–5833. [CrossRef] [PubMed]
137. Chatgilialoglu, C.; Ferreri, C.; Krokidis, M.G.; Masi, A.; Terzidis, M.A. On the relevance of hydroxyl radical to purine DNA damage. *Free Radic. Res.* **2021**, *55*, 384–404. [CrossRef]
138. Bergeron, F.; Auvre, F.; Radicella, J.P.; Ravanat, J.-L. HO$^{\bullet}$ radicals induce an unexpected high proportion of tandem base lesions refractory to repair by DNA glycosylases. *Proc. Natl. Acad. Sci. USA* **2010**, *107*, 5528–5533. [CrossRef]

Disclaimer/Publisher's Note: The statements, opinions and data contained in all publications are solely those of the individual author(s) and contributor(s) and not of MDPI and/or the editor(s). MDPI and/or the editor(s) disclaim responsibility for any injury to people or property resulting from any ideas, methods, instructions or products referred to in the content.